

Conditional canonical correlation estimation based on covariates with random forests

Cansu Alakus^{1,*}, Denis Larocque^{1,†}, Sébastien Jacquemont^{3,4}, Fanny Barlaam⁴, Charles-Olivier Martin⁴, Kristian Agbogba⁴, Sarah Lippé^{2,4}, and Aurélie Labbe^{1,†}

¹Department of Decision Sciences, HEC Montréal, Montréal, QC H3T 2A7, Canada

²Department of Psychology, Université de Montréal, Montréal, QC H3T 1J4, Canada

³Department of Pediatrics, Université de Montréal, Montréal, QC H3T 1C5, Canada

⁴CHU Sainte-Justine Research Center, Université de Montréal, Montréal, QC H3T 1C5, Canada

Abstract

Investigating the relationships between two sets of variables helps to understand their interactions and can be done with canonical correlation analysis (CCA). However, the correlation between the two sets can sometimes depend on a third set of covariates, often subject-related ones such as age, gender, or other clinical measures. In this case, applying CCA to the whole population is not optimal and methods to estimate conditional CCA, given the covariates, can be useful. We propose a new method called Random Forest with Canonical Correlation Analysis (RFCCA) to estimate the conditional canonical correlations between two sets of variables given subject-related covariates. The individual trees in the forest are built with a splitting rule specifically designed to partition the data to maximize the canonical correlation heterogeneity between child nodes. We also propose a significance test to detect the global effect of the covariates on the relationship between two sets of variables. The performance of the proposed method and the global significance test is evaluated through simulation studies that show it provides accurate canonical correlation estimations and well-controlled Type-1 error. We also show an application of the proposed method with EEG data.

*Corresponding author. E-mail: cansu.alakus@hec.ca

†After the first author, A Labbe and D Larocque are (equally) the main contributors of this article.

1 Introduction

Multi-view data denotes many kinds of data that provide information about a subject from multiple sources. For example, in biomedical studies, the collection of data may include subject-related covariates (e.g. age, gender, medical history), DNA sequencing, transcriptomics (e.g. mRNA, microRNA, RNA sequencing) and proteomics for a single subject (Network *et al.*, 2012; Consortium *et al.*, 2012). As another example, in functional neuroimaging, we may have subject-related covariates (e.g. age, gender, intracranial volume (ICV)), brain imaging data, and cognitive measurements for subjects (Fratello *et al.*, 2017). Integration of multiple feature sets and investigating the relationships between them may help to understand their interactions and obtain more meaningful interpretations. Studying the integration of multiple feature sets requires statistical and machine-learning tools which include methods for dimension reduction, clustering, classification, and association studies for multi-view data integration (see Sun (2013); Meng *et al.* (2016); Min *et al.* (2017); Li *et al.* (2018) for comprehensive reviews).

Canonical correlation analysis (CCA), firstly introduced in Hotelling (1936), is a multivariate statistical method that analyzes the relationship between two multivariate data sets, X and Y . CCA searches for linear combinations of each of the two data sets, Xa and Yb , having maximum correlation. In CCA, the components Xa and Yb are called canonical variates and their correlations are the canonical correlations. CCA is a two-view data integration tool. It was later generalized to data with more than two views (Kettenring, 1971). There are some extensions of CCA for under-determined data sets through regularized CCA (Vinod, 1976; Cruz-Cano and Lee, 2014), for sparse data sets through sparse-CCA (Witten *et al.*, 2009; Hardoon and Shawe-Taylor, 2011) and for nonlinear relationships through generalized CCA (Melzer *et al.*, 2001), deep CCA (Andrew *et al.*, 2013), kernel CCA (KCCA) (Akaho, 2001) and non-parametric CCA (NCCA) (Michaeli *et al.*, 2016). Although very flexible, all these methods suppose that the relationship between the two sets of variables is constant for all subjects, which is not always the case in practice. For example, hundred of gene-environment studies have shown that gene effects on diseases are modulated by environmental factors (Caspi and Moffitt, 2006; Hunter, 2005; Ma *et al.*, 2011). In the field of neuroscience, age and gender are known to interact with brain-behaviour correlations (Davis *et al.*, 2008; Li *et al.*, 2010) and this should be accounted for in the analyses. In this paper, we focus on CCA and specifically on extending it to account for a subject-related covariate effect on the correlation.

There are several ways to account for subject-related covariates in multi-view data analysis. They can be treated as one of the views (Hanna *et al.*, 2010; Li and Jung, 2017; Moser *et al.*, 2018; Mihalik *et al.*, 2020) or they can be used to identify subgroups in the data while analyzing the relationships between other views. Recently, Choi *et al.* (2020) proposed a recursive partitioning approach, namely correlation tree, to identify homogeneous correlated subgroups within data. In their work, the data consists of a set of subject-related covariates Z (e.g. age, gender, education) and two univariate continuous variables X and Y which are assumed to be correlated. The correlation tree method grows a decision tree with covariates to identify subgroups of subjects with different correlations between the two univariate variables. A simple illustration of this approach is shown in Figure 1 with a single split of the decision tree. In this example, the overall correlation between X and Y is $\rho = 0.329$. However, this hides the fact that the subgroup with $Z_1 > 0.011$ has a much higher correlation of $\rho_R = 0.741$ while the other subgroup $Z_1 \leq 0.011$ has almost no correlation ($\rho_L = 0.018$). Such a situation can be modeled in practice with a regression model including an interaction effect between X and Z , but the situation is not as straightforward when both Y and X are multivariate and when the interaction pattern with Z is complex enough to not be captured efficiently by a single tree. Therefore, the goal of this paper is to propose a novel way to estimate the canonical correlations between two sets of multivariate variables X and Y , depending on Z , using a random forests framework.

Random forest is an ensemble method which contains many decision trees. It is a powerful prediction method due to its ability to limit over-fitting. Moreover, random forests can be seen as a way to find nearest neighbor observations that are close to the one we want to predict (Hothorn *et al.*, 2004; Lin and Jeon, 2006; Moradian *et al.*, 2017, 2019; Roy and Larocque, 2020; Tabib and Larocque, 2020). Each tree in the proposed random forest framework is built with a new splitting rule designed to produce child nodes with maximum difference in the canonical correlation between X and Y . For a new observation with subject-related covariate values z^* , the proposed random forest provides a set of similar observations from the training data set that will be used to compute a canonical correlation estimate given z^* . Moreover, we propose a significance test to detect the global effect of Z on the relationship between X and Y .

This paper is organized as follows. In Section 2, we describe the proposed method, global significance test and variable importance measure. In Section 3, simulation study results for accuracy evaluation and global effect of covariates are presented to show the performance of the method. A real data example is provided in Section 4, followed by

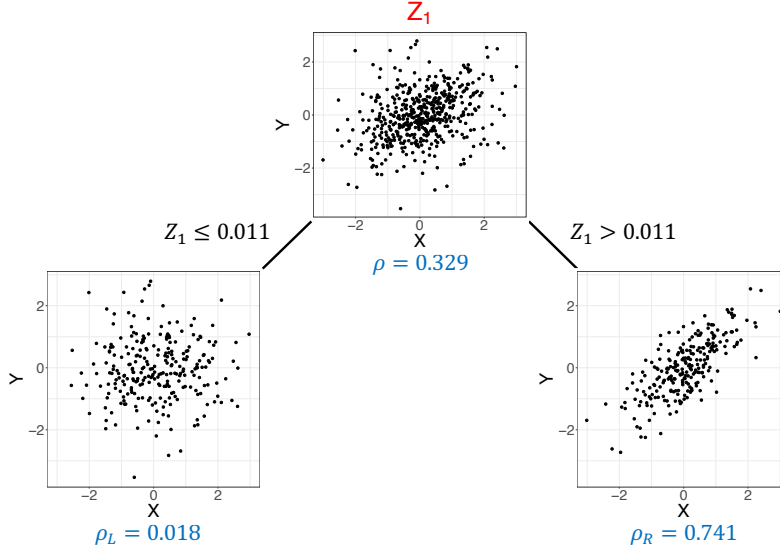


Figure 1: Example of a dataset (X, Y) where the correlation between X and Y depends on a covariate Z_1 . This can be captured by a single split of the decision tree.

concluding remarks in Section 5.

2 Proposed method

In this section, we describe the proposed method in detail.

2.1 Canonical correlation analysis (CCA)

Canonical correlation analysis (CCA), firstly introduced in Hotelling (1936), seeks vectors of $a \in R^p$ and $b \in R^q$, given two mean centered multivariate data sets $X \in R^{n \times p}$ and $Y \in R^{n \times q}$, such that Xa and Yb are maximally linearly correlated. We can formulate the problem as finding the coefficients (a^*, b^*) such that:

$$(a^*, b^*) = \operatorname{argmax}_{a, b} \operatorname{corr}(Xa, Yb), \quad (1)$$

where

$$\operatorname{corr}(Xa, Yb) = \frac{a^T \Sigma_{XY} b}{\sqrt{a^T \Sigma_{XX} a} \sqrt{b^T \Sigma_{YY} b}},$$

where Σ_{XX} and Σ_{YY} are the covariance matrices of X and Y , respectively, and Σ_{XY} is the cross-covariance matrix. Since rescaling a and b does not affect $\text{corr}(Xa, Yb)$, we can add the constraints $a^T \Sigma_{XX} a = 1$, $b^T \Sigma_{YY} b = 1$ to the maximization problem (1). There are several ways to solve the CCA problem, such as solving standard or generalized eigenvalue problems (Hotelling, 1936; Haroon *et al.*, 2004; Bach and Jordan, 2002), using alternating least squares regression (Branco *et al.*, 2005; Wilms and Croux, 2015) and using singular value decomposition (Healy, 1957; Ewerbring *et al.*, 1990).

2.2 Tree growing process

We use an unsupervised random forest based on the set of covariates Z to find subgroups of observations with similar canonical correlations between X and Y . This random forest consists of many unsupervised decision trees with a specialized splitting criterion. The tree growing process follows the CART approach (Breiman *et al.*, 1984). The basic idea of tree growing with CART is to select the best split at each parent node among all possible splits to obtain the purest child nodes. Assume we want to split a parent node with n_P observations into two child nodes, namely left and right nodes. To split a node, all possible splits are evaluated with the selected splitting criterion. A split value for each split point is calculated by using the observations in the parent node. Then, the best split is selected among all possible splits. The CART algorithm evaluates all possible splits to decide the split variable and split point. In random forests, instead of evaluating all possible splits, the best split search is limited to a randomly selected subset of covariates. Splitting continues until all nodes become terminal nodes.

Since the goal is to find subgroups of subjects with distinct canonical correlations, we propose a splitting rule that will seek to increase the canonical correlation heterogeneity as fast as possible (Athey *et al.*, 2019; Moradian *et al.*, 2017; Tabib and Larocque, 2020). Define ρ_L and ρ_R as the canonical correlation estimations of the left and right nodes, respectively. The proposed splitting criterion is

$$\sqrt{n_L n_R} * |\rho_L - \rho_R|, \quad (2)$$

where n_L and n_R are the left and right node sizes, respectively. The best split among all possible splits is the one that maximizes (2). Choi *et al.* (2020) propose a similar criterion without the $\sqrt{n_L n_R}$ term among one of three possible splitting criteria for their correlation tree method.

2.3 Random forest and estimation of canonical correlation for new observations

The previous section describes the splitting criterion and tree growing process for a single tree. The final canonical correlations are estimated with a random forest. Random forest (Breiman, 2001) is a data-driven weight generator. For example, for a continuous outcome, we can represent random forest predictions for a new observation as a weighted average of the true responses such as $\hat{\delta}^{new} = \sum_{i=1}^N \hat{w}_i (c^{new}) o_i$, where \hat{w}_i are the predicted weights from the random forest, c^{new} are the covariates of the new observation, and o_i are the observed outcomes (Hothorn *et al.*, 2004; Lin and Jeon, 2006).

A slightly different representation of these weights was presented in Moradian *et al.* (2017) and later used in Moradian *et al.* (2019), Roy and Larocque (2020) and Tabib and Larocque (2020). For a new observation, we form a set of observations which includes the training observations that are in the same terminal nodes as the new observation. Roy and Larocque (2020) called this set of observations the Bag of Observations for Prediction (BOP). We can define BOP for a new observation c^{new} as

$$BOP(c^{new}) = \bigcup_{b=1}^B S_b^{new},$$

where S_b^{new} is the set of training observations that are in the same node as c^{new} in the b^{th} tree. Any desired measure can be obtained by using the constructed BOP. In this paper, we use the BOP idea to estimate the canonical correlations for the new observations. Once we train the random forest, we can estimate the correlation for any new observation. In our problem, for a new observation with covariates z^{new} , we firstly form $BOP(z^{new})$. Then, we apply canonical correlation analysis for X and Y with the observations in $BOP(z^{new})$, to compute the canonical correlation estimation $\hat{\rho}(z^{new})$.

We can estimate CCA components only if the sample size, n , is larger than $(p + q)$. In fact, if $n < (p + q)$, the first $(p + q - n)$ canonical correlations will be exactly one and uninformative (Pezeshki *et al.*, 2004). When $n > (p + q)$, although we can estimate the CCA correlations, overfitting can still be a problem. As the sample size in proportion to $(p + q)$ increases, the likelihood of overfitting decreases. During the tree building process, the number of observations in the nodes are getting smaller as we move down in the tree. When the sample size of a node in proportion to a fixed total number of X and Y variables is close to one, we are more likely to overfit. Therefore, we need to control the minimum

sample size in the nodes and we do it using the `nodesize` feature of random forests.

2.4 Global significance test

For each tree grown in the forest, the proposed method uses the covariate space to identify groups of observations with similar canonical correlations. By doing so, we might be tempted to assume that the set of covariates is indeed relevant to distinguish between canonical correlations. However, this might not be the case and we propose a hypothesis test to evaluate the global effect of the covariates on the canonical correlation. The unconditional canonical correlation between X and Y can be found by computing CCA using the whole sample. If there is a global effect of Z on such correlations, the estimated conditional canonical correlations with the proposed method should be significantly different from the unconditional canonical correlation. We perform the following statistical significance test for the null hypothesis

$$H_0 : \rho(X, Y|Z) = \rho_{CCA}(X, Y), \quad (3)$$

where $\rho(X, Y|Z)$ is the conditional canonical correlation between X and Y given Z , and $\rho_{CCA}(X, Y)$ is the unconditional CCA correlation in the population.

Before describing the global significance test, we will describe how to estimate canonical correlations for the training data using out-of-bag (OOB) observations. We train a random forest with B trees using the training observations. Each tree $b = \{1, \dots, B\}$ is built with the selected random bootstrap sample, i.e. inbag observations (IB^b), that contains approximately 63% distinct observations from the original sample. The remaining training observations are the OOB observations for that tree, namely OOB^b , and they are not used for building the b^{th} tree. After training a random forest with B trees, we have (IB^b, OOB^b) sets for each tree. The estimation of canonical correlation with OOB observations is described in Algorithm 1 for a training set with a sample of size n . Basically, for a given training observation, the canonical correlation is estimated with the BOP, but using only the trees for which that observation is OOB.

The proposed global significance test is described in Algorithm 2. Firstly, we apply CCA to all X and Y to compute the unconditional canonical correlation, which is the root node correlation, say ρ_{root} . Then, we apply the proposed method for X, Y, Z and estimate the canonical correlations for each training observation, $\hat{\rho}(z_i)$, by using OOB observations as described in Algorithm 1. Finally, we compute the global test statistic with

Algorithm 1 Estimation of canonical correlation for a training observation z_i with OOB observations

```

1: for  $i=1,\dots,n$  do
2:   for  $b=1,\dots,B$  do
3:     if  $z_i \in OOB^b$  then
4:       Find the terminal node of  $z_i$  at tree  $b$ , say  $d$ 
5:        $BOP_{oob}(z_i) = BOP_{oob}(z_i) \cup IB_d^b(z_i)$  (where  $IB_d^b(z_i)$  is the inbag observations
        that are in the same terminal node  $d$  as  $z_i$ )
6:     end if
7:   end for
8:   Apply CCA for  $X$  and  $Y$  with the observations in  $BOP_{oob}(z_i)$  to find the estimated
        canonical correlation  $\hat{\rho}(z_i)$ 
9: end for

```

$$T = \frac{1}{n} \sum_{i=1}^n (\hat{\rho}(z_i) - \rho_{root})^2. \quad (4)$$

The global test statistic is the mean squared difference between the unconditional canonical correlation between X and Y , and the estimated canonical correlations with the proposed method. It measures how far the estimated canonical correlations are spread out from the unconditional canonical correlation between X and Y . The larger T is, the more evidence against H_0 we have. We perform a permutation test under the null hypothesis (3) by randomly permuting rows of Z . For each permuted Z , we compute the global test statistic (4) and estimate a p -value with

$$p = \frac{1}{R} \sum_{r=1}^R I(T'_r > T), \quad (5)$$

where T'_r is the test statistic for the r^{th} permuted Z and R is the total number of permutations. If the p -value is less than the pre-specified significance level α , we reject the null hypothesis (3).

Algorithm 2 Global permutation test for covariates' effects

- 1: Compute CCA for X and Y in the root node, say ρ_{root}
 - 2: Train RF with X, Y, Z
 - 3: Compute estimated canonical correlations with Algorithm 1, say $\hat{\rho}(z_i)$
 - 4: Compute test statistic with $T = \frac{1}{n} \sum_{i=1}^n (\hat{\rho}(z_i) - \rho_{root})^2$
 - 5: **for** $r = 1 : R$ **do**
 - 6: Permute rows of Z , say Z_r
 - 7: Train RF with X, Y, Z_r
 - 8: Compute estimated canonical correlations with Algorithm 1, say $\hat{\rho}'_r(z_i)$
 - 9: Compute test statistic with $T'_r = \frac{1}{n} \sum_{i=1}^n (\hat{\rho}'_r(z_i) - \rho_{root})^2$
 - 10: **end for**
 - 11: Approximate the permutation p -value with (5)
 - 12: Reject the null hypothesis when $p < \alpha$. Otherwise, do not reject the null hypothesis.
-

2.5 Variable importance

Random forests use OOB samples to construct variable importance (VIMP) measures by evaluating the average change in prediction accuracy. However, we do not have a true response variable since the problem is unsupervised by nature. Therefore, we use the predicted values to compute any VIMP measures we want from existing packages. The idea is that we are measuring the importance of the variables by using a regression forest to reproduce the canonical correlation estimations we obtained from our method. Hence, the VIMP measures reflect the predictive power of the variables on the estimated canonical correlations. Therefore, higher value of VIMP measure implies higher importance for the estimation of canonical correlations. We propose a two-step process to estimate VIMP measures; see Section 3.1 of the Supplementary Material for details.

2.6 Implementation

We utilised the custom splitting feature of the `randomForestSRC` package (Ishwaran and Kogalur, 2020) to implement our splitting criterion in the tree building process. We have developed an R package called `RFCCA`. The package is currently available on Github <https://github.com/calakus/RFCCA> and is under review for CRAN.

3 Simulations

Evaluating the performance of the proposed method with a real data set is not possible since the true relationships between X and Y with varying Z are typically unknown. Hence, we perform a simulation study with a known data generation process (DGP) to show the performance of our method. We first describe the DGP used in the simulation study. Next, we construct scenarios to validate the proposed global significance test. Since we know the true correlations, we can evaluate the accuracy of the correlation estimations. We can also evaluate the estimated importance ranking of the covariates since we know the set of covariates that are effectively related to the relationship between X and Y , and the ones that are redundant.

3.1 DGP

Assume we want to generate a data set with $X \in R^{n \times p}$, $Y \in R^{n \times q}$ and $Z \in R^{n \times r}$ where n is the sample size. We firstly generate the covariates Z according to a standard multivariate normal distribution with an equicorrelated covariance matrix, that is from $N(0, \Sigma_Z)$ where $\Sigma_Z = (1 - \rho_z)\mathbf{I}_r + \rho_z\mathbf{J}_r$, \mathbf{I}_r and \mathbf{J}_r are $r \times r$ identity matrix and matrix of ones, respectively. Then, the true correlation between Xa and Yb for each observation i , $\rho(z_i)$, is generated with the following logit model

$$\rho(z_i) = \frac{1}{1 + \exp(-(\beta_0 + \sum_{l=1}^r \beta_l z_{il} + z_{i1}^2))},$$

where β_0 is the intercept parameter and β_l are the weights for the Z variables. In the simulations, we set all β_l to be $1/r$.

Next, we generate the X and Y coefficients for CCA, a and b in (1) respectively, with the following two linear equations:

$$\begin{aligned} a_{ij} &= \max\{0, (1 - s_x \times \rho(z_i) \times j)\} \quad \forall j = \{1, 2, \dots, p\}, \\ b_{ik} &= \max\{0, (1 - s_y \times \rho(z_i) \times k)\} \quad \forall k = \{1, 2, \dots, q\}, \end{aligned}$$

where s_x and s_y are some slope parameters to be defined. Note that according to these equations, the X and Y variables have a descending order of relative importance. Also, we may set some coefficients to be 0 with an appropriate choice of s_x and s_y , in order to have redundant covariates that are not directly related to the canonical correlations.

Finally, for each observation i , we generate the X and Y variables with a multivariate normal distribution $N(0, \Sigma_i)$, where $\Sigma_i = \begin{pmatrix} \Sigma_X & \Sigma_{XY}^i \\ \Sigma_{YX}^i & \Sigma_Y \end{pmatrix}$, $\Sigma_X = (1 - \rho_x)\mathbf{I}_p + \rho_x\mathbf{J}_p$, $\Sigma_Y = (1 - \rho_y)\mathbf{I}_q + \rho_y\mathbf{J}_q$ and $\Sigma_{XY}^i = \rho(z_i)\Sigma_X a_i b_i^T \Sigma_Y$. See Section 4 of the Supplementary Material for examples of sample distributions with different parameter settings.

3.2 Simulation design

3.2.1 Evaluation of the power of the global significance test

In order to evaluate the effect of Z , we consider four scenarios where two of them are under the null hypothesis (3) and the other two are under the alternative hypothesis. For all scenarios, we generate X and Y with two levels of CCA correlation defined to be low (0.3) and high (0.6). For the first scenario (case 1 under H_0), these levels represent the population correlation. For the other three scenarios, they represent the mean sample correlation. We generate the data sets for these scenarios as follows:

1. H_0 (case 1): We generate 5 X , 5 Y with a constant population canonical correlation and 10 Z variables which are all independent and following a standard normal distribution. In this case, the correlation between X and Y is independent of Z and we are therefore under the null hypothesis.
2. H_0 (case 2): We first generate 5 X , 5 Y and 5 Z with the proposed DGP. Then, we replace the Z set with 10 independent Z variables generated with a standard normal distribution. In this case, the correlation between X and Y varies with some of the Z variables but those Z variables are not available in the training set. Hence, although the correlation between X and Y is a function of covariates, these covariates are not part of the training set. Therefore, we are again under the null hypothesis.
3. H_1 (without noise): We generate 5 X , 5 Y and 5 Z with the proposed DGP, and the covariates are available in the training set. In this case, the correlation between X and Y varies with all Z variables.
4. H_1 (with noise): We generate 5 X , 5 Y and 5 Z with the proposed DGP and we add 5 independent Z variables to the covariates' training set. In this case, the correlation between X and Y varies with some of the Z variables.

Parameters	Low CCA correlation	High CCA correlation
(p, q)	(1,1), (5,5), (10,10)	(1,1), (5,5), (10,10)
(r, r^{noise})	(1,5), (5,5), (10,5)	(1,5), (5,5), (10,5)
(ρ_x, ρ_y, ρ_z)	(0.3, 0.3, 0.1)	(0.3, 0.3, 0.1)
(β_0, β_l)	$(-2, \frac{1}{r})$	$(-0.3, \frac{1}{r})$
(s_x, s_y)	(0.7, 0.4)	(0.4, 0.3)

Table 1: DGP parameter settings for accuracy evaluation simulations. We consider two levels of average CCA correlation: low (0.3) and high (0.6).

Each of the scenarios above are repeated under the low and high correlation settings, which leads to a total of 8 scenarios to investigate. We also investigate how the performance of the proposed method varies with the training sample sizes, and we use $n_{train} = \{200, 300, 500, 1000, 1500\}$. The number of permutations in the permutation test is set to 500 and each scenario is repeated 500 times. Type-1 error is estimated as the proportion of rejection in the scenarios simulated under H_0 . Similarly, we estimate power as the proportion of rejection in the scenarios simulated under H_1 .

For each replication of the simulation, we obtain an estimated p -value from the permutation test. If the p -value is less than the significance level $\alpha = 0.05$, we reject the null hypothesis. The proportion of rejection is then calculated over the 500 replications.

3.2.2 Accuracy evaluation

We perform a simulation study to evaluate the accuracy of the method for estimating the canonical correlation. Table 1 presents the DGP parameter settings for these simulations. We generate Z with $(r, r^{noise}) = \{(1, 5), (5, 5), (10, 5)\}$ where r and r^{noise} are the number of important and noise Z variables, respectively. We generate X and Y with $(p, q) = \{(1, 1), (5, 5), (10, 10)\}$ where p and q are the number of X and Y variables, respectively. We use training sample sizes of $n_{train} = \{100, 200, 300, 500, 1000, 5000\}$. Also, we consider two values parameter `nodesize` that controls the size of the trees: `nodesize` = $3 \times (p + q)$ and `nodesize` = $6 \times (p + q)$. Overall, these combinations produce 216 settings (2 mean CCA correlation levels \times 3 Z dimensionality \times 3 X and Y dimensionality \times 6 training sample sizes \times 2 `nodesize` levels). Each setting is repeated 100 times for a total of 216,000 runs. In each run, we generate an independent test set of new observations with $n_{test} = 1000$.

We evaluate the performance with the mean absolute errors (MAE), given by

$$MAE = \frac{1}{n_{test}} \sum_{i=1}^{n_{test}} |\hat{\rho}(z_i) - \rho(z_i)|, \quad (6)$$

where $\hat{\rho}(z_i)$ is the estimated canonical correlation and $\rho(z_i)$ is the true correlation for the i^{th} test observation with covariates z_i . Smaller values of the MAE show better performance. We use ordinary CCA, without covariates, as a simple benchmark method. In this case, we let ρ_{train} be the training sample estimated canonical correlation with CCA. This value is used as the correlation estimation for all new observations from the test set.

3.3 Results

3.3.1 Global significance test

Figure 2 illustrates the estimated Type-1 error for different training sample sizes for both H_0 case 1 and 2. In the first and second columns, we have results for the low and high correlated data sets, respectively. In H_0 scenarios, we expect the Type-1 error to be close to the significance level ($\alpha = 0.05$). As can be seen from plots, the Type-1 error is well controlled in both cases. Figure 3 illustrates the power of the test. In all scenarios and as expected, the power is increasing with the sample size. However, adding noise covariates slightly decreases the power when the sample size is small. As the sample size increases, the power is not affected by the presence of noise covariates.

3.3.2 Accuracy evaluation

We provide a summary of the results in Figures 4 and 5 which present the average MAE over the 100 repetitions when `nodesize` = $3 \times (p + q)$ for the low and high correlation settings, respectively. The plots illustrate the change in MAE with increasing training sample size for different r and (p, q) settings. In our simulations, selecting `nodesize` as $3 \times (p + q)$ leads to smaller or very similar MAE results (see Section 5 of the Supplementary Material for the performance evaluation results for the two levels of `nodesize`). As can be seen from both figures, the proposed method and the benchmark have a similar performance, with a slight advantage for the proposed method in some cases with high correlation, when $n = 100$. When the sample size increases, the MAE of both methods decrease but markedly faster for the proposed method. Hence, in the settings considered,

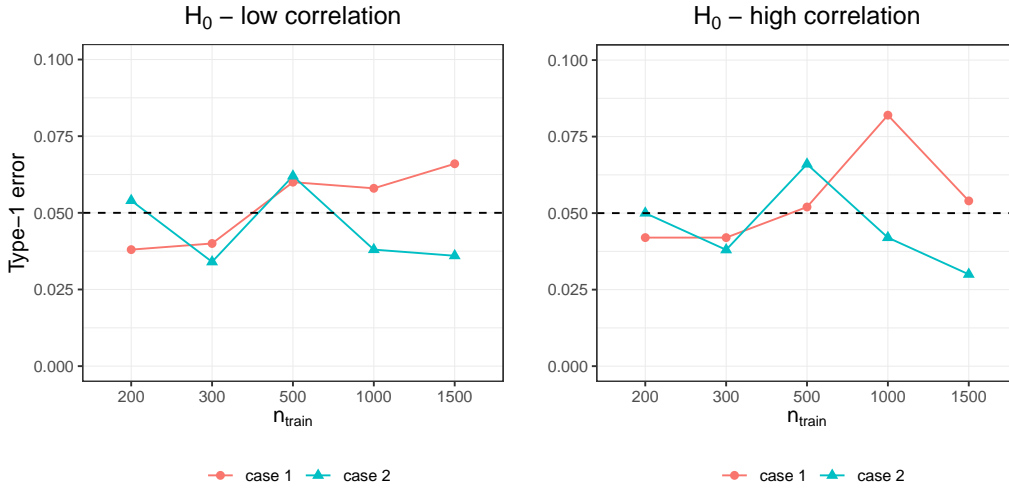


Figure 2: Global significance test results for H_0 cases. In case 1 the correlation between X and Y is not varying with Z and in case 2 the correlation between X and Y is varying with some of the Z variables but those Z variables are not used in the training set. Left and right plots are for low and high correlated data sets, respectively. Dashed line represents the significance level of $\alpha = 0.05$.

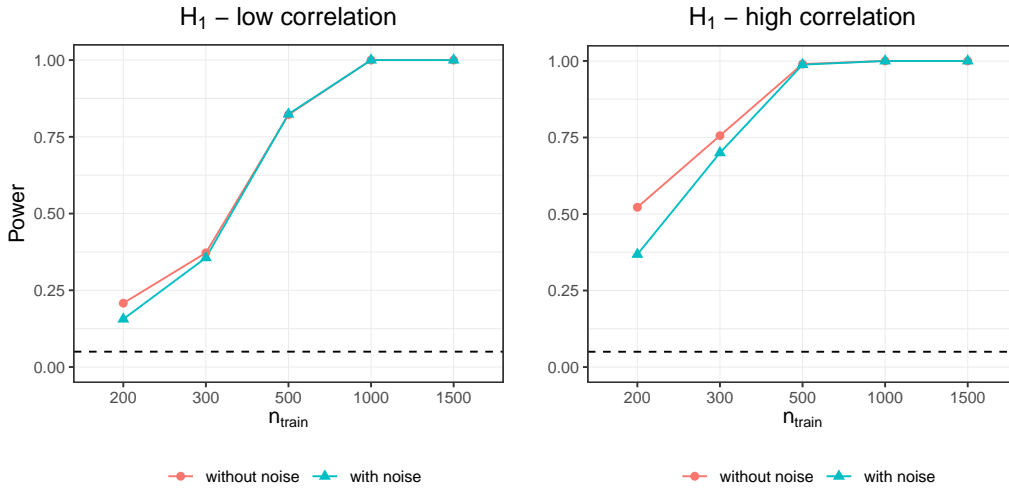


Figure 3: Global significance test results for H_1 scenarios. In without noise case, we have only important covariates for the varying correlation between X and Y and in with noise case we have additional noise covariates. Left and right plots are for low and high correlated data sets, respectively. Dashed line represents the significance level of $\alpha = 0.05$.

a small sample size of 100 is not sufficient for the proposed method to improve over the ordinary CCA. But when the sample size increases, the proposed method successfully exploits the covariates to provide more accurate estimations of the canonical correlation, the relative gain being more important in the high correlation settings.

3.3.3 Variable importance

For the variable importance, we evaluate if the estimated VIMP measures tend to rank the important variables first. In all scenarios for performance evaluation, we include noise covariates. Figures presenting the average rank, from the estimated VIMP measures, for the important variables group and noise variables group, for both low and high correlated data sets can be found in Section 3.2 of the Supplementary Material. The most important variable (the one with the highest VIMP measure) has rank 1. As ranks increases, variable importance decreases. In almost all settings, the important variables have smaller average ranks than noise variables. Only in a few settings when $n_{train} = 100$, we have close average ranks for the important and noise variables.

4 Real data example

Electroencephalogram (EEG) measures neuronal activity. Electrodes are distributed on the scalp to record ongoing electrical fields coming from assemblies of pyramidal neurons situated in the cortex. The signal is composed of continuous variation in rhythms that can be spectrally decomposed over time through time and frequency analyses. Oscillations at different frequency bands have been found to be interdependent (Samiee and Baillet, 2017). Only a handful of studies have assessed the effect of age on cross-frequency interdependencies. However, its relationship with the intellectual level is still unknown.

In this study, 241 participants between 3 and 64 years old (113 male/128 female) and with performance IQ (pIQ) within [56, 129] and verbal IQ (vIQ) within [50, 127] were submitted to broadband noises of 50ms at 1Hz while the EEG signal was recorded using the 128 electrode EGI system (auditory evoked potentials, AEPs) (see Lippé *et al.* (2009) for paradigm details). Variation in IQ levels is due to 99 participants presenting with a copy number variation (CNV). The data collection and preprocessing steps are described in the Supplementary Material (Section 6). After applying the time-frequency (TF) and inter-trial coherence (ITC) analyses, we have two variables of interest, power, and phase-

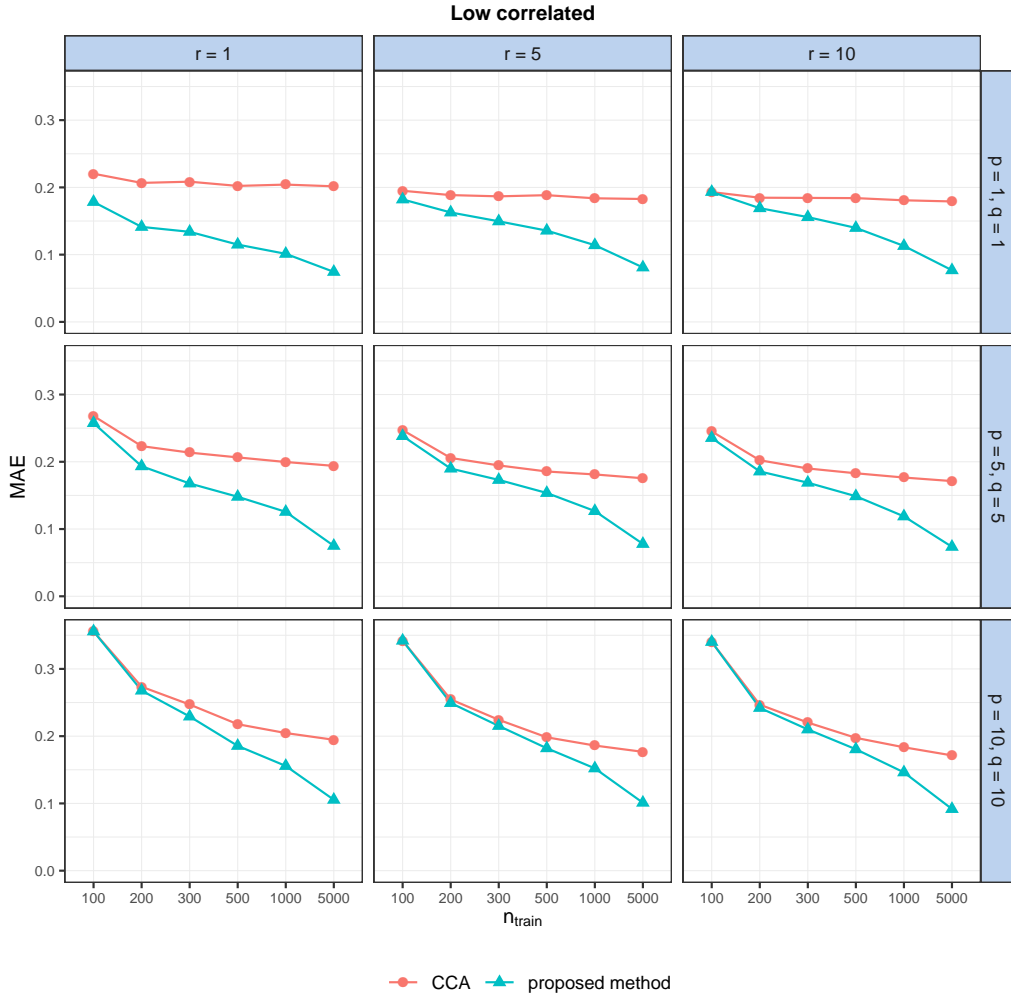


Figure 4: Performance evaluation results for low correlated data sets when $\text{nodesize} = 3 \times (p + q)$. $r^{\text{noise}} = 5$ in all settings. CCA is the benchmark method. Smaller values of MAE are better.

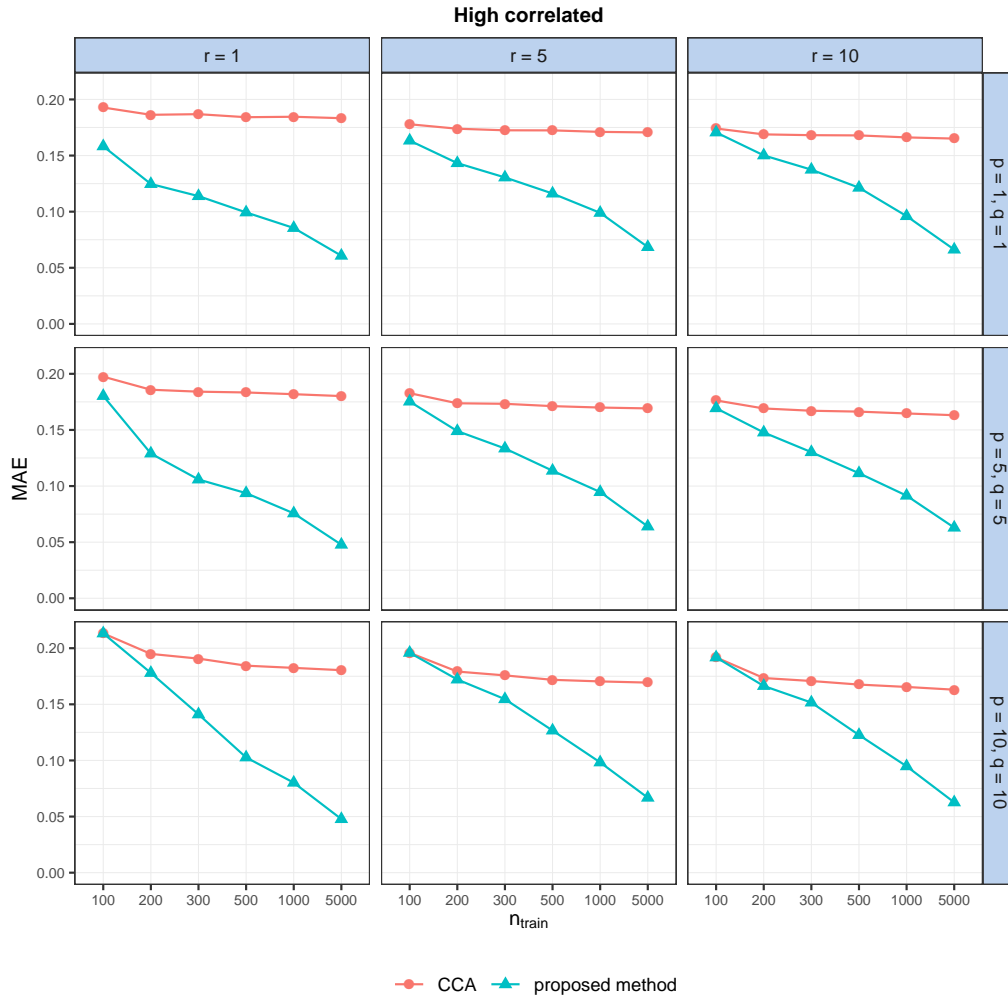


Figure 5: Performance evaluation results for high correlated data sets when $\text{nodesize} = 3 \times (p + q)$. $r^{\text{noise}} = 5$ in all settings. CCA is the benchmark method. Smaller values of MAE are better.

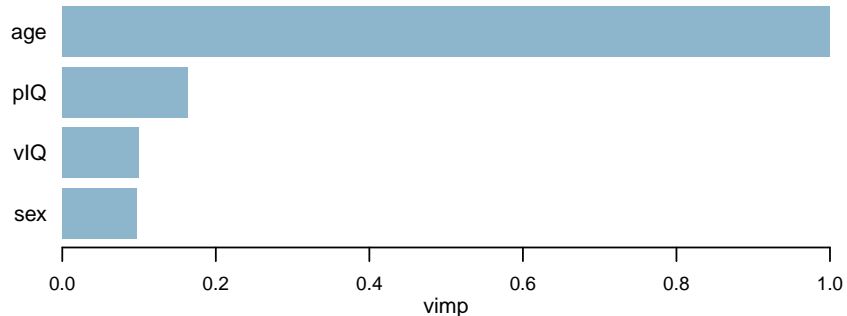


Figure 6: Variable importance measures computed with the proposed method.

locking value (PLV) for each window. The time and frequency windows of interest are selected to assess low and high-frequency dependencies. In particular, the three windows for PLV are in theta waves with 3–5 Hz (100–300 ms), 3–10 Hz (4–400 ms), and 3–10 Hz (100–300 ms), and the window for power is in gamma wave with 30–50 Hz (50–150 ms).

We want to analyze the association between the PLV variables in theta waves (X , $p = 3$) and power in gamma wave (Y , $q = 1$) in the mid-frontal (MF) region which is composed of Fz-Fcz in addition to four surrounding electrodes. We apply the proposed method with the subject-related covariates age, sex, pIQ, vIQ (Z , $r = 4$) to investigate the correlation between PLV and power for the sample with $n = 241$. We first perform the global significance test to evaluate the global effect of the covariates. Using 500 permutations, the estimated p -value with (5) is 0.004 and we reject the null hypothesis (3), indicating that the canonical correlation varies significantly with the covariates. Next, we apply the proposed method to the data and obtain the canonical correlation estimations. Figure 6 presents the VIMP showing that age is the most important variable followed by pIQ, vIQ and sex.

We also use SHAP values (Lundberg and Lee, 2017) to gain additional insights. SHAP values show how much each variable contributes, either positively or negatively, to the individual predictions. Since the problem is unsupervised, as in the VIMP computation, we use the predicted correlations to compute the SHAP values, using Lundberg *et al.* (2020). Figure 7 presents the summary plot. The covariates are ordered in the y -axis of the plot according to their global importance showing that we obtain the same ranking as with the VIMP and thus that age is again the most important variable. The insights from this exploratory analysis fall into the expectations. Age, or brain maturation, is

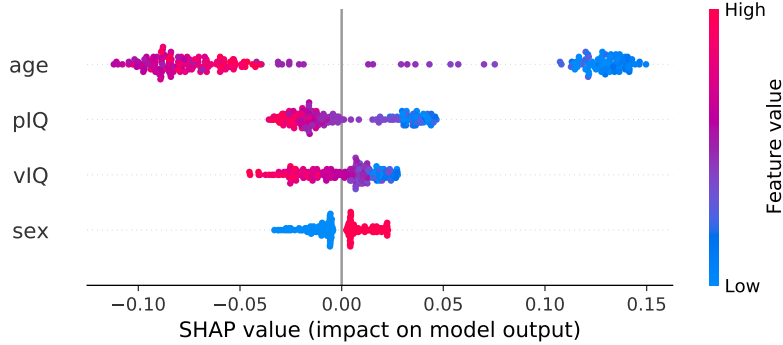


Figure 7: SHAP summary plot.

accompanied by important neurofunctional modifications that are reflected in the theta-gamma band co-variations. The demonstration of a positive correlation and a strong contribution to the model in children and adolescents (3 to 20 years of age) is concordant with current brain development literature (Cho *et al.*, 2015). Intellectual quotient, the hallmark of cognitive abilities, is found to be the second most contributive variable to the theta-gamma co-variation. Current literature focused on the theta-gamma coupling links with performances on specific cognitive tasks (Aleksichuk *et al.*, 2016), and showed positive correlations. This result points to the relevance of theta-gamma co-variation in the context of abnormal neurodevelopment (Port *et al.*, 2019).

Left plot in Figure 8 shows the main effect of age on the predictions. We can see how age’s attributed importance changes as its value varies. The attributed importance is on the y -axis. The points are colored according to the predicted correlation. We can interpret this plot as the impact of age on correlation is positive and high for subjects younger than 20. Then it drops sharply reaching 0 (no impact) around 25 (note that we do not have observations around 20 and the results should be interpreted cautiously in that region). It then continues to decrease in the negative direction, meaning the impact increases until the beginning of the 30’s where it stabilizes with a slight increase afterwards (i.e. a decreasing impact).

Right plot in Figure 8 presents the interaction effect between sex and piQ (see Figure 10 in the Supplementary Material for the interaction effect between sex and viQ). We see that the impact increases as we move away from the average IQ. The impact of the interaction on the theta-gamma co-variation is positive for high IQ females and negative for low IQ females. The opposite is observed in males.

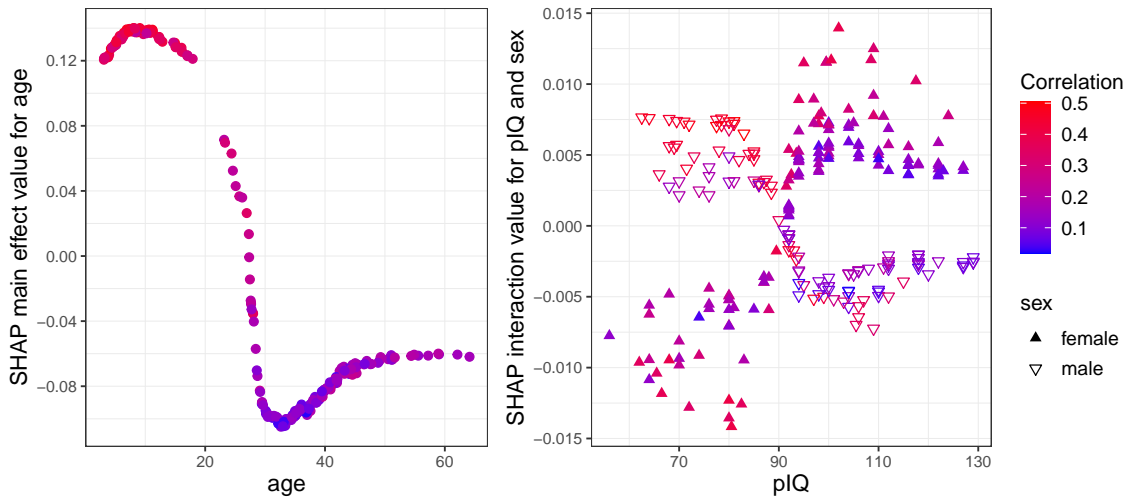


Figure 8: (Left) SHAP main effect values for age. (Right) SHAP interaction values for sex and pIQ.

5 Concluding remarks

In this paper, we study and propose a novel random forest method to estimate the canonical correlations between two sets of variables depending on a set of subject-related covariates. The trees of the forest are built with a new splitting rule designed to form child nodes with maximum difference in the canonical correlation between the two multivariate data sets. Random forest is used to build Bag of Observations for Prediction (BOP) which can be used to compute any desired measure. We use the BOP to estimate the correlations with canonical correlation analysis for the new observations. The proposed method is flexible to various extensions. One of them is to use CCA variants such as sparse CCA (Witten *et al.*, 2009) and regularized CCA (Vinod, 1976; Leurgans *et al.*, 1993) for final canonical correlation estimation for a new observation using the constructed BOP. Another one is to build trees with alternative splitting rules such as $n_L \rho_L^2 + n_R \rho_R^2$ where ρ_L and ρ_R are left and right canonical correlation estimations and n_L and n_R are left and right node sizes, respectively. It would be interesting to investigate these extensions as a future work.

We also propose a global significance test to evaluate the global effect of the subject-related covariates and a way to compute variable importance measures. It would also be interesting to study the statistical significance of variable importance measures. However, a limitation of the proposed method is the computational time. Computing CCA for

$X \in R^{n \times p}$ and $Y \in R^{n \times q}$ has a time complexity $O(n(p^2 + q^2))$ where $n > p + q$. For each node split in each tree of the forest, we compute CCA for left and right nodes which brings a lot of CCA computations. Therefore, testing the statistical significance of variable importance of covariates with permutation test has a great computational cost.

For simulations and real data analysis, we used the default parameter settings for `randomForestSRC` except the number of trees and the `nodesize` argument. We train random forests with 200 trees and `nodesize= 3 × (p + q)`. In `randomForestSRC`, default sampling for random forest training, unlike bootstrapping as in the original random forest algorithm, is sampling without replacement (sub-sampling). We obtain smaller trees with sub-sampling than bootstrapping when we set large `nodesize`. One can improve the performance of the algorithm with bootstrapping in return for increased computational time. Moreover, by default, only 10 random splits are considered at each candidate splitting variable to increase the speed. Evaluating all possible splits could also improve the performance.

Funding

This research was supported by the Natural Sciences and Engineering Research Council of Canada (NSERC), and by Fondation HEC Montréal.

References

- Akaho, S. (2001). A kernel method for canonical correlation analysis. In *In Proceedings of the International Meeting of the Psychometric Society (IMPS2001)*. Springer-Verlag.
- Alekseichuk, I. *et al.* (2016). Spatial working memory in humans depends on theta and high gamma synchronization in the prefrontal cortex. *Current Biology*, **26**(12), 1513–1521.
- Andrew, G. *et al.* (2013). Deep canonical correlation analysis. In *International conference on machine learning*, pages 1247–1255.
- Athey, S. *et al.* (2019). Generalized random forests. *The Annals of Statistics*, **47**(2), 1148–1178.
- Bach, F. R. and Jordan, M. I. (2002). Kernel independent component analysis. *Journal of machine learning research*, **3**(Jul), 1–48.
- Branco, J. A. *et al.* (2005). Robust canonical correlations: A comparative study. *Computational Statistics*, **20**(2), 203–229.
- Breiman, L. (2001). Random forests. *Machine learning*, **45**(1), 5–32.
- Breiman, L. *et al.* (1984). *Classification and regression trees*. CRC press.
- Caspi, A. and Moffitt, T. E. (2006). Gene–environment interactions in psychiatry: joining forces with neuroscience. *Nature Reviews Neuroscience*, **7**(7), 583–590.
- Cho, R. Y. *et al.* (2015). Development of sensory gamma oscillations and cross-frequency coupling from childhood to early adulthood. *Cerebral cortex*, **25**(6), 1509–1518.
- Choi, D. *et al.* (2020). A recursive partitioning approach for subgroup identification in brain–behaviour correlation analysis. *Pattern Analysis and Applications*, **23**(1), 161–177.
- Consortium, E. P. *et al.* (2012). An integrated encyclopedia of dna elements in the human genome. *Nature*, **489**(7414), 57–74.
- Cruz-Cano, R. and Lee, M.-L. T. (2014). Fast regularized canonical correlation analysis. *Computational Statistics & Data Analysis*, **70**, 88–100.

- Davis, S. W. *et al.* (2008). Que pasa? the posterior–anterior shift in aging. *Cerebral cortex*, **18**(5), 1201–1209.
- Ewerbring, L. M. *et al.* (1990). Canonical correlations and generalized svd: applications and new algorithms. In *Advances in Parallel Computing*, volume 1, pages 37–52. Elsevier.
- Fratello, M. *et al.* (2017). Multi-view ensemble classification of brain connectivity images for neurodegeneration type discrimination. *Neuroinformatics*, **15**(2), 199–213.
- Hanna, F. *et al.* (2010). Anthropometric and demographic correlates of dual-axis swallowing accelerometry signal characteristics: a canonical correlation analysis. *Dysphagia*, **25**(2), 94–103.
- Hardoon, D. R. and Shawe-Taylor, J. (2011). Sparse canonical correlation analysis. *Machine Learning*, **83**(3), 331–353.
- Hardoon, D. R. *et al.* (2004). Canonical correlation analysis: An overview with application to learning methods. *Neural computation*, **16**(12), 2639–2664.
- Healy, M. (1957). A rotation method for computing canonical correlations. *Mathematics of Computation*, **11**(58), 83–86.
- Hotelling, H. (1936). Relations between two sets of variates. *Biometrika*, **28**(3/4), 321–377.
- Hothorn, T. *et al.* (2004). Bagging survival trees. *Statistics in medicine*, **23**(1), 77–91.
- Hunter, D. J. (2005). Gene–environment interactions in human diseases. *Nature Reviews Genetics*, **6**(4), 287–298.
- Ishwaran, H. and Kogalur, U. (2020). *Fast Unified Random Forests for Survival, Regression, and Classification (RF-SRC)*. R package version 2.9.3.
- Kettenring, J. R. (1971). Canonical analysis of several sets of variables. *Biometrika*, **58**(3), 433–451.
- Leurgans, S. E. *et al.* (1993). Canonical correlation analysis when the data are curves. *Journal of the Royal Statistical Society: Series B (Methodological)*, **55**(3), 725–740.
- Li, G. and Jung, S. (2017). Incorporating covariates into integrated factor analysis of multi-view data. *Biometrics*, **73**(4), 1433–1442.

- Li, T. *et al.* (2010). Gender-specific hemodynamics in prefrontal cortex during a verbal working memory task by near-infrared spectroscopy. *Behavioural brain research*, **209**(1), 148–153.
- Li, Y. *et al.* (2018). A review on machine learning principles for multi-view biological data integration. *Briefings in bioinformatics*, **19**(2), 325–340.
- Lin, Y. and Jeon, Y. (2006). Random forests and adaptive nearest neighbors. *Journal of the American Statistical Association*, **101**(474), 578–590.
- Lippé, S. *et al.* (2009). Electrophysiological study of auditory development. *Neuroscience*, **164**(3), 1108–1118.
- Lundberg, S. M. and Lee, S.-I. (2017). A unified approach to interpreting model predictions. In *Advances in neural information processing systems*, pages 4765–4774.
- Lundberg, S. M. *et al.* (2020). From local explanations to global understanding with explainable ai for trees. *Nature Machine Intelligence*, **2**(1), 2522–5839.
- Ma, S. *et al.* (2011). Varying coefficient model for gene–environment interaction: a non-linear look. *Bioinformatics*, **27**(15), 2119–2126.
- Melzer, T. *et al.* (2001). Nonlinear feature extraction using generalized canonical correlation analysis. In *International Conference on Artificial Neural Networks*, pages 353–360. Springer.
- Meng, C. *et al.* (2016). Dimension reduction techniques for the integrative analysis of multi-omics data. *Briefings in bioinformatics*, **17**(4), 628–641.
- Michaeli, T. *et al.* (2016). Nonparametric canonical correlation analysis. In *International Conference on Machine Learning*, pages 1967–1976.
- Mihalik, A. *et al.* (2020). Multiple holdouts with stability: Improving the generalizability of machine learning analyses of brain–behavior relationships. *Biological psychiatry*, **87**(4), 368–376.
- Min, S. *et al.* (2017). Deep learning in bioinformatics. *Briefings in bioinformatics*, **18**(5), 851–869.

- Moradian, H. *et al.* (2017). L1 splitting rules in survival forests. *Lifetime data analysis*, **23**(4), 671.
- Moradian, H. *et al.* (2019). Survival forests for data with dependent censoring. *Statistical methods in medical research*, **28**(2), 445–461.
- Moser, D. A. *et al.* (2018). Multivariate associations among behavioral, clinical, and multimodal imaging phenotypes in patients with psychosis. *JAMA psychiatry*, **75**(4), 386–395.
- Network, C. G. A. *et al.* (2012). Comprehensive molecular portraits of human breast tumours. *Nature*, **490**(7418), 61.
- Pezeshki, A. *et al.* (2004). Empirical canonical correlation analysis in subspaces. In *Conference Record of the Thirty-Eighth Asilomar Conference on Signals, Systems and Computers, 2004.*, volume 1, pages 994–997. IEEE.
- Port, R. G. *et al.* (2019). Children with autism spectrum disorder demonstrate regionally specific altered resting-state phase–amplitude coupling. *Brain Connectivity*, **9**(5), 425–436.
- Roy, M.-H. and Larocque, D. (2020). Prediction intervals with random forests. *Statistical Methods in Medical Research*, **29**(1), 205–229.
- Samiee, S. and Baillet, S. (2017). Time-resolved phase-amplitude coupling in neural oscillations. *NeuroImage*, **159**, 270–279.
- Sun, S. (2013). A survey of multi-view machine learning. *Neural computing and applications*, **23**(7-8), 2031–2038.
- Tabib, S. and Larocque, D. (2020). Non-parametric individual treatment effect estimation for survival data with random forests. *Bioinformatics*, **36**(2), 629–636.
- Vinod, H. D. (1976). Canonical ridge and econometrics of joint production. *Journal of econometrics*, **4**(2), 147–166.
- Wilms, I. and Croux, C. (2015). Sparse canonical correlation analysis from a predictive point of view. *Biometrical Journal*, **57**(5), 834–851.
- Witten, D. M. *et al.* (2009). A penalized matrix decomposition, with applications to sparse principal components and canonical correlation analysis. *Biostatistics*, **10**(3), 515–534.

Supplementary Material for Conditional canonical correlation estimation based on covariates with random forests

1 Motivating examples

1.1 Example with univariate X and Y

We generated a data set with $Z = (Z_1, \dots, Z_{10}) \in R^{n \times 10}$, $X \in R^{n \times 1}$ and $Y \in R^{n \times 1}$ where $n = 500$, $Z_i \sim N(0, 1) \forall i = \{1, 2, \dots, 10\}$ and $(X, Y) \sim MVN(0, \Sigma)$ where $\Sigma = \begin{pmatrix} 1 & \rho \\ \rho & 1 \end{pmatrix}$. The correlation between X and Y is a function of Z_1 given by

$$\rho = \begin{cases} 0 & Z_1 \leq 0 \\ 0.8 & Z_1 > 0 \end{cases}$$

where ρ is the population correlation between X and Y . The sample correlation between X and Y , as a function of Z_1 , is

$$r(X, Y) = \begin{cases} 0.017 & Z_1 \leq 0 \\ 0.737 & Z_1 > 0 \end{cases}$$

whereas the sample correlation between all X and Y is 0.329. Our aim is to identify the two groups of observations having the most different correlation. After applying the proposed method with a single tree and a single split, we have two groups of observations. Figure 1 illustrates the single split of the method. The observations are grouped according to their Z_1 values, the first group has $Z_1 \leq 0.011$ and the second group has $Z_1 > 0.011$. The correlation between X and Y in those two groups are respectively 0.018 and 0.741. Hence, the proposed method was able to identify the two groups.

1.2 Example with multivariate X and Y

As a second example, now with multivariate X and Y , we have a data set with $Z \in R^{n \times 10}$, $X \in R^{n \times 2}$ and $Y \in R^{n \times 2}$ where $n = 500$, $Z_i \sim N(0, 1) \forall i = \{1, 2, \dots, 10\}$. The canonical

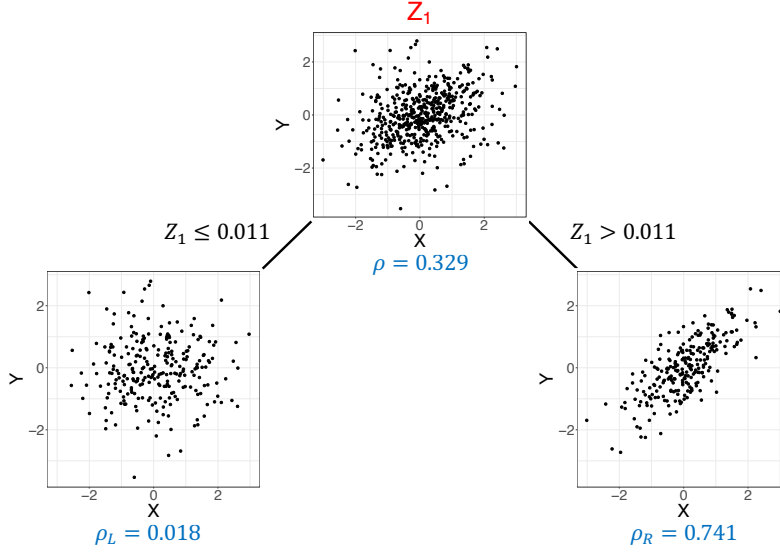


Figure 1: Illustration for the example, single split of a single decision tree.

correlation between X and Y is a function of Z_1

$$\rho_{CCA} = \begin{cases} 0.2 & Z_1 \leq 0 \\ 0.8 & Z_1 > 0 \end{cases}$$

where ρ_{CCA} is the population CCA correlation between X and Y . The sample CCA correlations between X and Y as a function of Z_1 is

$$r_{CCA}(X, Y) = \begin{cases} 0.237 & Z_1 \leq 0 \\ 0.785 & Z_1 > 0 \end{cases}$$

whereas the sample CCA correlation between all X and Y is 0.535. Again, after applying the proposed method with a single tree and single split, we have two groups of observations. The observations are grouped according to their Z_1 values, the first group has $Z_1 \leq 0.014$ and the second group has $Z_1 > 0.014$. The CCA correlation between X and Y in those two groups are respectively 0.237 and 0.785. Thus, again, the proposed method was able to identify the two groups.

2 Computing canonical correlations

Canonical correlation analysis, firstly introduced in Hotelling (1936), seeks vectors of $a \in R^p$ and $b \in R^q$ for two multivariate data sets $X \in R^{n \times p}$ and $Y \in R^{n \times q}$ such that Xa and Yb are maximally linearly correlated. We can formulate the problem

$$(a^*, b^*) = \operatorname{argmax}_{a,b} \operatorname{corr}(Xa, Yb) \quad (7)$$

where

$$\operatorname{corr}(Xa, Yb) = \frac{a^T \Sigma_{XY} b}{\sqrt{a^T \Sigma_{XX} a} \sqrt{b^T \Sigma_{YY} b}},$$

and where Σ_{XX} and Σ_{YY} are the covariance matrices of X and Y , respectively, and Σ_{XY} is the cross-covariance matrix. The choice of rescaling of a and b does not affect the $\operatorname{corr}(Xa, Yb)$, so we can add the constraints $a^T \Sigma_{XX} a = 1$, $b^T \Sigma_{YY} b = 1$ to the maximization problem (7).

In Hotelling (1936), the CCA solution is based on two similar-looking equations

$$(\Sigma_{YX} \Sigma_{XX}^{-1} \Sigma_{XY} - \rho^2 \Sigma_{YY})y = 0 \quad (8)$$

$$(\Sigma_{XY} \Sigma_{YY}^{-1} \Sigma_{YX} - \rho^2 \Sigma_{XX})x = 0 \quad (9)$$

where Σ_{YX} is the transpose of Σ_{XY} . We can find canonical correlations and (a^*, b^*) by solving two standard eigenvalue problems. Basically, eigenvalues of (8) and (9) are the same and equal to the squared canonical correlations.

In addition to solving standard eigenvalue problem, there are some alternative ways to solve CCA. We can solve the generalized eigenvalue problem (Hardoon *et al.*, 2004; Bach and Jordan, 2002). We can find the solution of CCA by alternating least squares regression (Branco *et al.*, 2005; Wilms and Croux, 2015). Alternatively, we can use singular value decomposition (SVD) to find the canonical correlations (Healy, 1957; Ewerbring *et al.*, 1990). In the SVD method, we firstly find the singular value decompositions of X and Y as

$$\begin{aligned} X &= U_X D_X V_X^T \\ Y &= U_Y D_Y V_Y^T \end{aligned}$$

where the columns of $U_X(U_Y)$ and the columns of $V_X(V_Y)$ are called the left and right singular vectors of $X(Y)$, respectively. Then, we can find the canonical correlations by finding the singular values of $U_X^T U_Y$. Overall, this method requires three singular value decompositions.

Another way to compute canonical correlations is to find the QR decomposition of X and Y and then apply SVD (Golub, 1969; Björck and Golub, 1973). The QR decomposition of X and Y are

$$\begin{aligned} X &= Q_X R_X \\ Y &= Q_Y R_Y \end{aligned}$$

where $Q_X^T Q_X = I_p$, $Q_Y^T Q_Y = I_q$, and R_X and R_Y are upper triangular matrices. Following this, we can express Σ_X and Σ_Y as

$$\begin{aligned} \Sigma_X &= X^T X \\ &= R_X^T Q_X^T Q_X R_X \\ &= R_X^T R_X \\ \Sigma_Y &= Y^T Y \\ &= R_Y^T Q_Y^T Q_Y R_Y \\ &= R_Y^T R_Y \end{aligned}$$

where $\Sigma_X = R_X^T R_X$ and $\Sigma_Y = R_Y^T R_Y$ are the Cholesky decompositions. The singular values of $Q_X^T Q_Y$, which are derived from

$$\begin{aligned} (R_X^T)^{-1} \Sigma_{XY} R_Y^{-1} &= (R_X^T)^{-1} R_X^T Q_X^T Q_Y R_Y R_Y^{-1} \\ &= Q_X^T Q_Y, \end{aligned}$$

are the canonical correlations. This method requires two QR decompositions and one singular value decomposition. Since QR decomposition for a matrix requires less computational work than computing SVD (Do Q, 2012), we utilise QR decomposition to compute canonical correlations in the implementation of our methods.

3 Variable importance

In this section, we explain computation of the variable importance for covariates in random forest framework and present the simulation results for the estimated variable importance.

3.1 Variable importance computation

The quantification of variable importance (VIMP) is important to assess relative importance of covariates. In the random forest framework, the mostly used VIMP idea proposed by Breiman (2001) is based on the increase in the prediction error when the link between the covariates and the response is broken by permuting out-of-bag (OOB) observations. In a regression setting with a set of covariates X and for a continuous response variable Y , VIMP for X_j can be computed as

$$VIMP(X_j) = \frac{1}{B} \sum_{b=1}^B (MSE(OOB_j^b) - MSE(OOB^b))$$

where OOB^b is the OOB sample of the b^{th} tree of the forest, OOB_j^b is the OOB sample of the b^{th} tree where the j^{th} covariate is randomly permuted and MSE stands for the mean squared error. The average over B trees gives the variable importance measure for X_j . Larger VIMP shows greater importance.

`randomForestSRC` uses the same idea of breaking the link between covariates and the response but with another way of permuting X_j as proposed in Ishwaran (2007). Instead of permuting OOB samples at each tree, during the tree growing process, observations in the parent node are assigned to child nodes at random or consistently to the other child node when the split variable is X_j . VIMP for X_j can be computed as

$$VIMP(X_j) = \frac{1}{B} \sum_{b=1}^B (MSE(\tilde{t}^b, OOB^b) - MSE(t^b, OOB^b)) \quad (10)$$

where t^b is the original b^{th} tree of the forest, \tilde{t}^b is the permuted b^{th} tree, and OOB^b is the OOB sample of the b^{th} tree.

Computing VIMP measure (10) requires the true response values for training observations. However, in this paper the problem is unsupervised by nature. Therefore, we propose a two-step process for VIMP computation. Firstly, we build a random forest with

the proposed splitting criterion for X , Y , Z and compute the estimated canonical correlations, $\hat{\rho}(z_i)$, as described in Algorithm 1 in the paper. Then, we use the $\hat{\rho}(z_i)$ estimations as a continuous response variable for the original covariates (Z) and we train a regression random forest. Finally, we use the VIMP measures from this random forest.

3.2 Simulation results for variable importance

As stated in Section 3.3.3 of the paper, Figures 2 and 3 present the average rank, from the estimated VIMP measures, for the important variables group and noise variables group, for low and high correlated data sets, respectively. The most important variable (the one with the highest VIMP measure) has rank 1. As ranks increases, variable importance decreases. We see that in almost all settings, the important variables have smaller average ranks than noise variables.

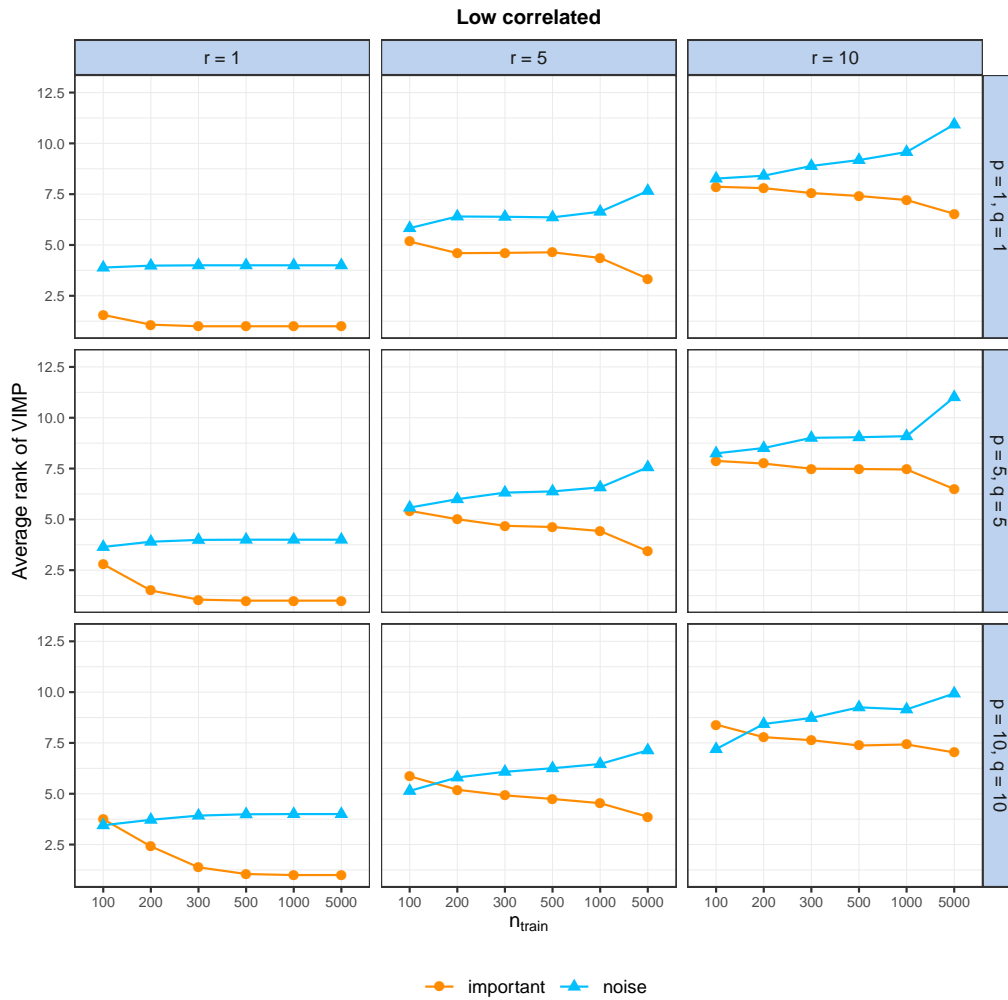


Figure 2: Average ranks from estimated VIMP measures for low correlated data sets when $n_{\text{nodesize}} = 3 \times (p + q)$. Smaller values of rank indicate a more important variable (the most important variable has rank 1).

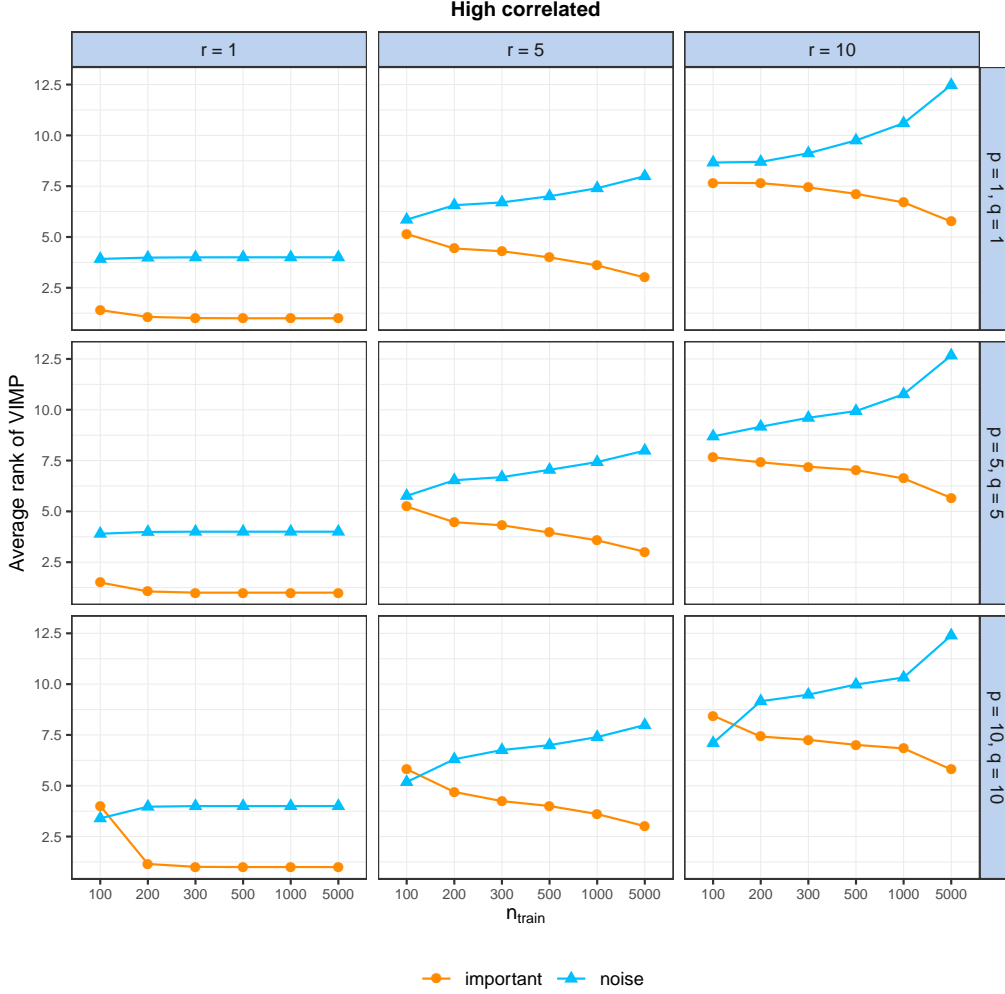


Figure 3: Average ranks from estimated VIMP measures for high correlated data sets when $n_{\text{nodesize}} = 3 \times (p + q)$. Smaller values of rank indicate a more important variable (the most important variable has rank 1).

4 Examples of sample distributions with DGP

Figures 4 and 5 show some examples for sample distributions with different parameter settings. See Section 3.1 of the paper for the explanation of DGP. Figure 4 and 5 correspond to the low and high correlated data settings with $n_{\text{train}} = 1000$ in the simulations for accuracy evaluation (Section 3.2.2 of the paper), respectively. The left plot in the figures is

the histogram of the generated sample. In the low correlated data setting (Figure 4), the mean and median correlations of the sample are 0.29 and 0.20, respectively. In the high correlated setting (Figure 5), the mean and median correlations of the sample are 0.61 and 0.57, respectively. The right plot in the figures is the ordered bar chart for the average of the coefficients within the X and Y sets over the sample. The selection of parameters s_x and s_y affects the coefficients of variables. In both low and high correlated settings, $s_x > s_y$ which result in faster decrease in generated X coefficients (*a*) compared to Y coefficients (*b*).

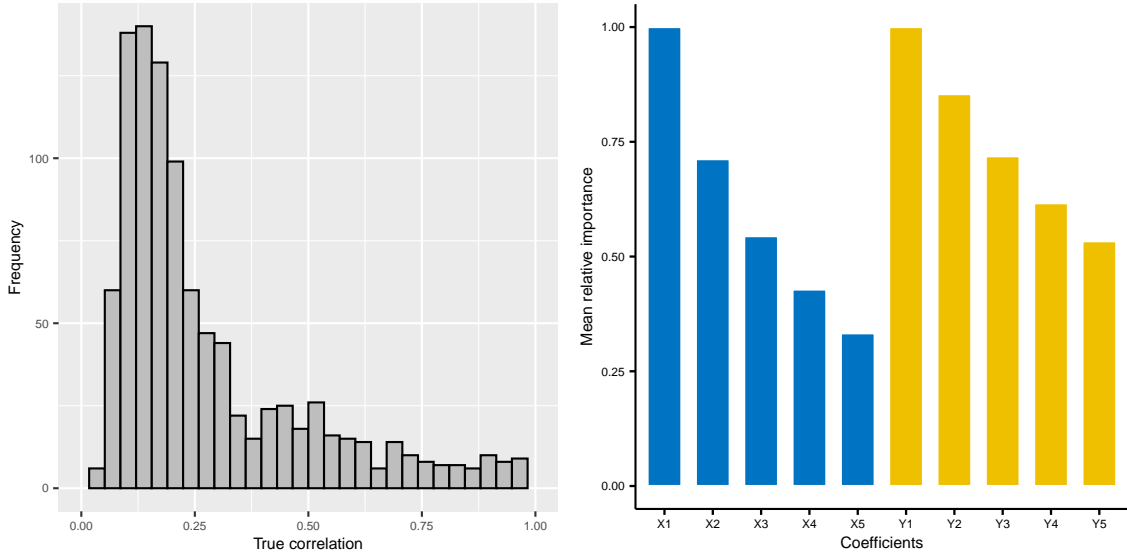


Figure 4: In this example, we have $5X, 5Y, 5Z$ variables and the sample size is 1000. The DGP parameters are $\beta_0 = -2$, $\rho_x = \rho_y = 0.3$, $\rho_z = 0.1$, $s_x = 0.7$, $s_y = 0.4$. The mean and median correlations are 0.29 and 0.20, respectively. This setting corresponds to the low correlated data set with $n_{train} = 1000$. (*left*) The sample distribution of correlations. (*right*) The ordered bar chart for the average of the coefficients within the X and Y sets over the sample.

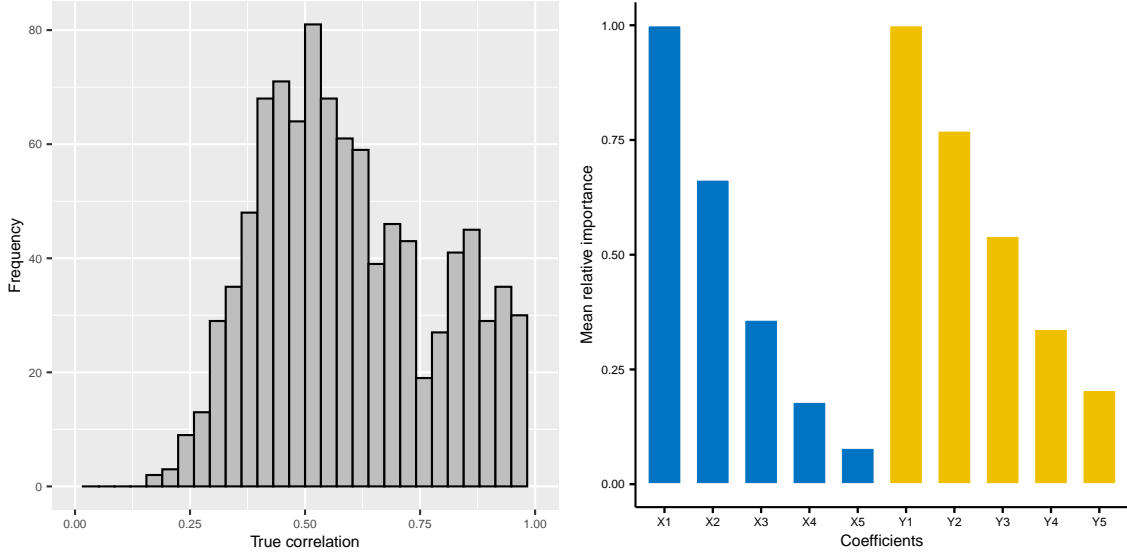


Figure 5: In this example, we have $5X, 5Y, 5Z$ variables and the sample size is 1000. The DGP parameters are $\beta_0 = -0.3$, $\rho_x = \rho_y = 0.3$, $\rho_z = 0.1$, $s_x = 0.4$, $s_y = 0.3$. The mean and median correlations are 0.61 and 0.57, respectively. This setting corresponds to the high correlated data set with $n_{train} = 1000$. (left) The sample distribution of correlations. (right) The ordered bar chart for the average of the coefficients within the X and Y sets over the sample.

5 Simulations results for accuracy evaluation

In this section, we present the detailed simulations results for accuracy evaluation. See Section 3.2.2 of the paper for the explanation of performance criterion.

5.1 Results for nodesize selection

Here we compare the performance of the proposed method with two levels of **nodesize**, $3 \times (p + q)$ and $6 \times (p + q)$, for low and high correlated data settings and $n_{train} = \{100, 200, 300, 500, 1000, 5000\}$. Figure 6 and 7 presents the average *MAE* over the 100 repetitions with each n_{train} for the low and high correlation settings, respectively. As mentioned in the paper, selecting **nodesize** as $3 \times (p + q)$ results in smaller or very similar *MAE* than $6 \times (p + q)$ in most of the scenarios. There are only a few scenarios such as low correlated data set with $r = 1$, $p = 10, q = 10$ and $n_{train} = 1000$ where **nodesize** =

$6 \times (p + q)$ has smaller *MAE* than $3 \times (p + q)$. As stated in Section 2.3, overfitting can still be a problem even when the sample size is larger than $(p + q)$. Hence, it is expected to decrease the risk of overfitting as increasing the `nodesize`. However, increasing `nodesize` results in random forests with smaller trees (fewer terminal nodes with many observations) which may cause bigger *BOPs* and underestimated canonical correlations. Therefore, it is better to set `nodesize` small but large enough to prevent overfitting.

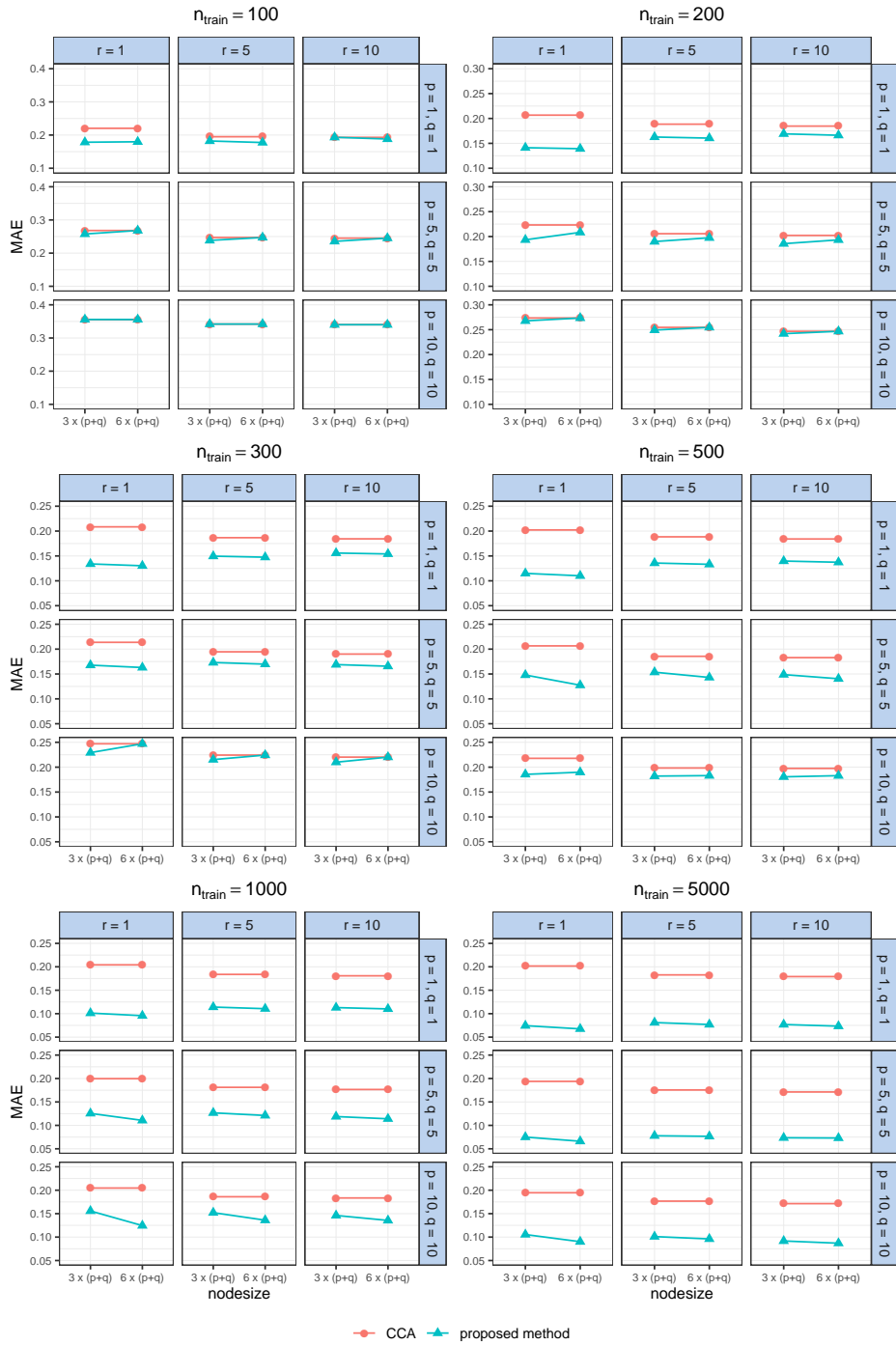


Figure 6: Performance evaluation results for low correlated data sets. CCA is the benchmark method. Smaller values of MAE are better.

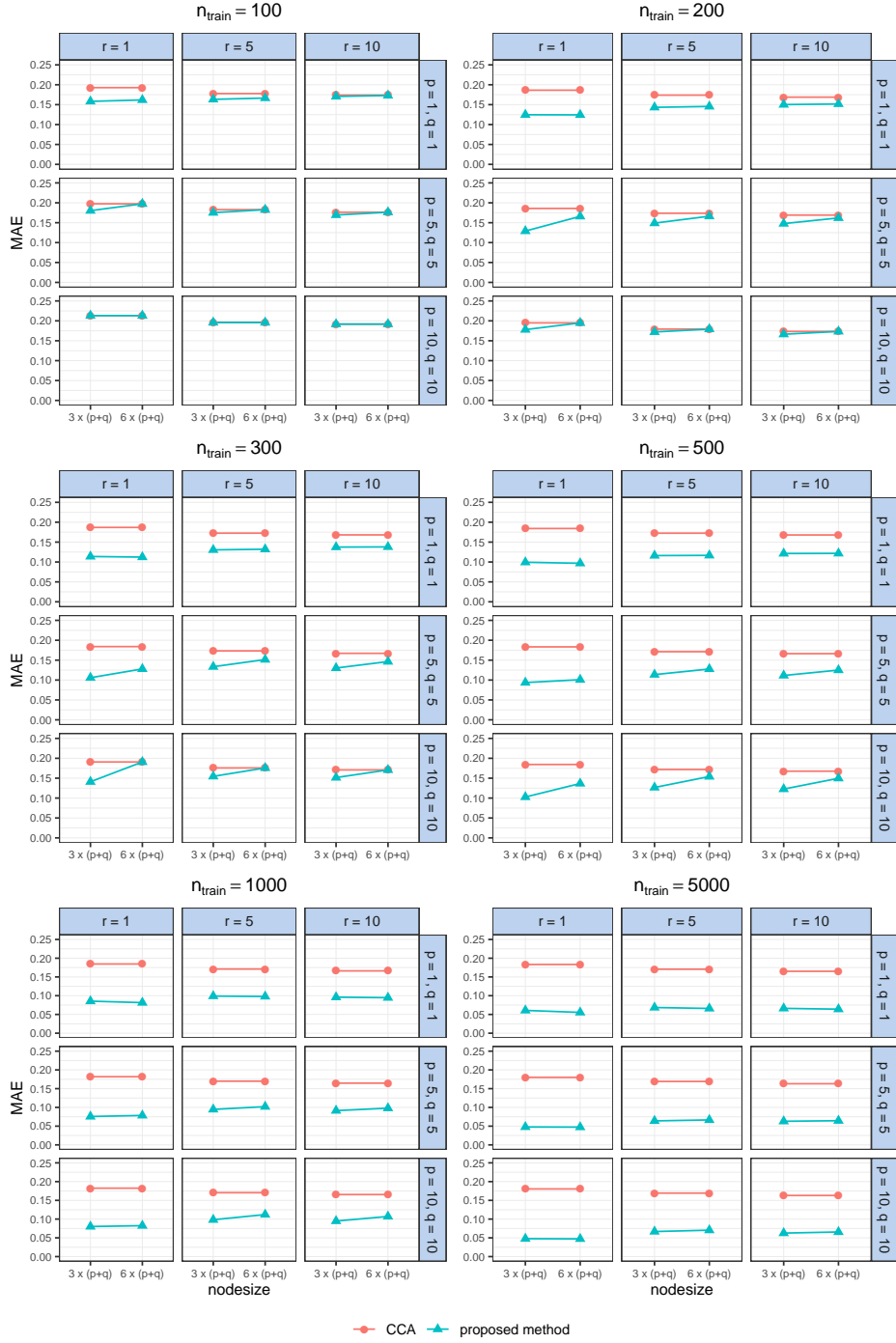


Figure 7: Performance evaluation results for high correlated data sets. CCA is the benchmark method. Smaller values of MAE are better.

5.2 Performance results for $\text{nodesize} = 6 \times (p + q)$

Figure 8 and 9 presents the average MAE over the 100 repetitions when $\text{nodesize} = 6 \times (p + q)$ for the low and high correlation settings, respectively. In fact, Figure 8 corresponds to Figure 4 in the paper and is represented here to be able to compare with the results of $\text{nodesize} = 3 \times (p + q)$. Similarly, Figure 9 corresponds to Figure 5 in the paper. As can be seen in Figure 8 and 9, MAE of the proposed method and the benchmark method are the same for $p = 10, q = 10$ when $n_{train} = \{100, 200, 300\}$. For this setting, $\text{nodesize} = 6 \times (10 + 10) = 120$ which results in no splits for $n_{train} = \{100, 200\}$. For $n_{train} = 300$, a single split can occur in trees with this nodesize . However, the BOP of a new observation may include all of the training observations due to randomness. Each tree of the forest is a stump and there is a high chance that the union of the training observations that are in the same terminal nodes as the new observation is equal to the set of training observations. Estimating canonical correlation with this BOP is the same as computing CCA for all X and Y . When the sample size is small, increasing the nodesize may cause underfitting.

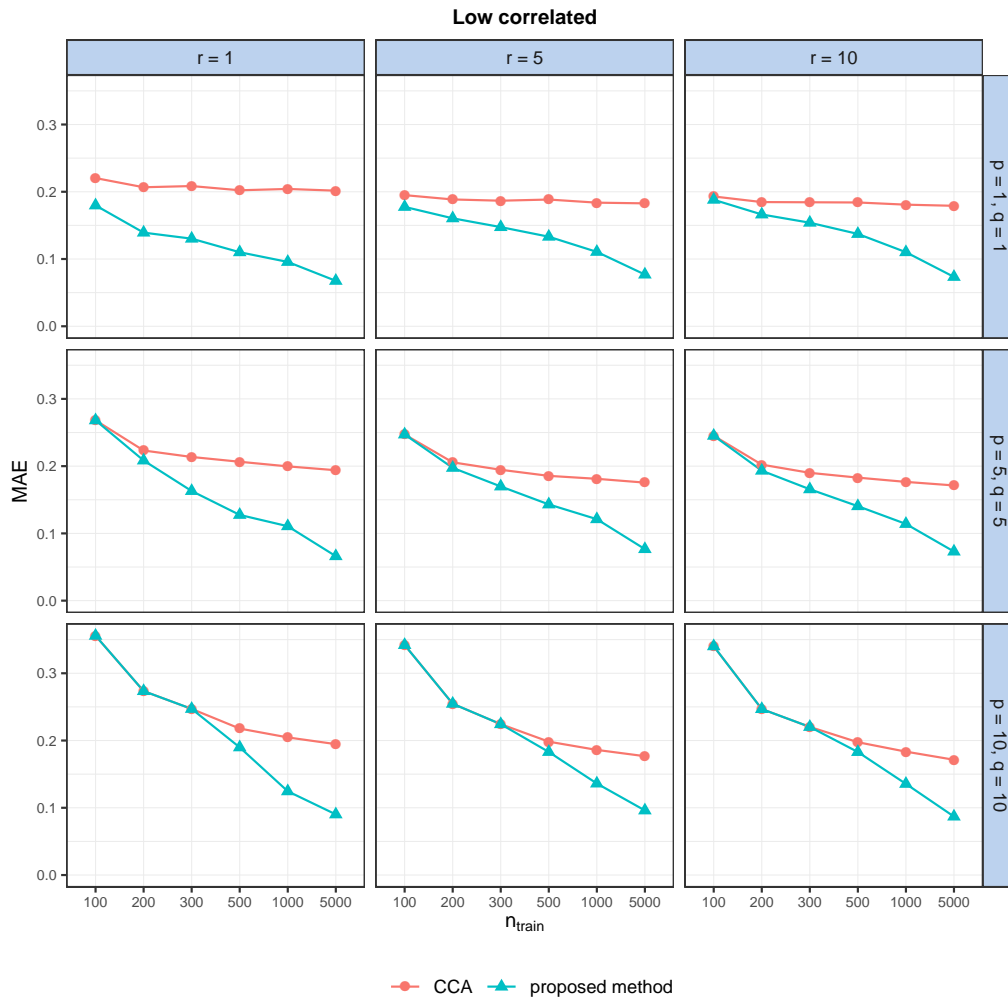


Figure 8: Performance evaluation results for low correlated data sets when $\text{nodesize} = 6 \times (p + q)$. CCA is the benchmark method. Smaller values of MAE are better.

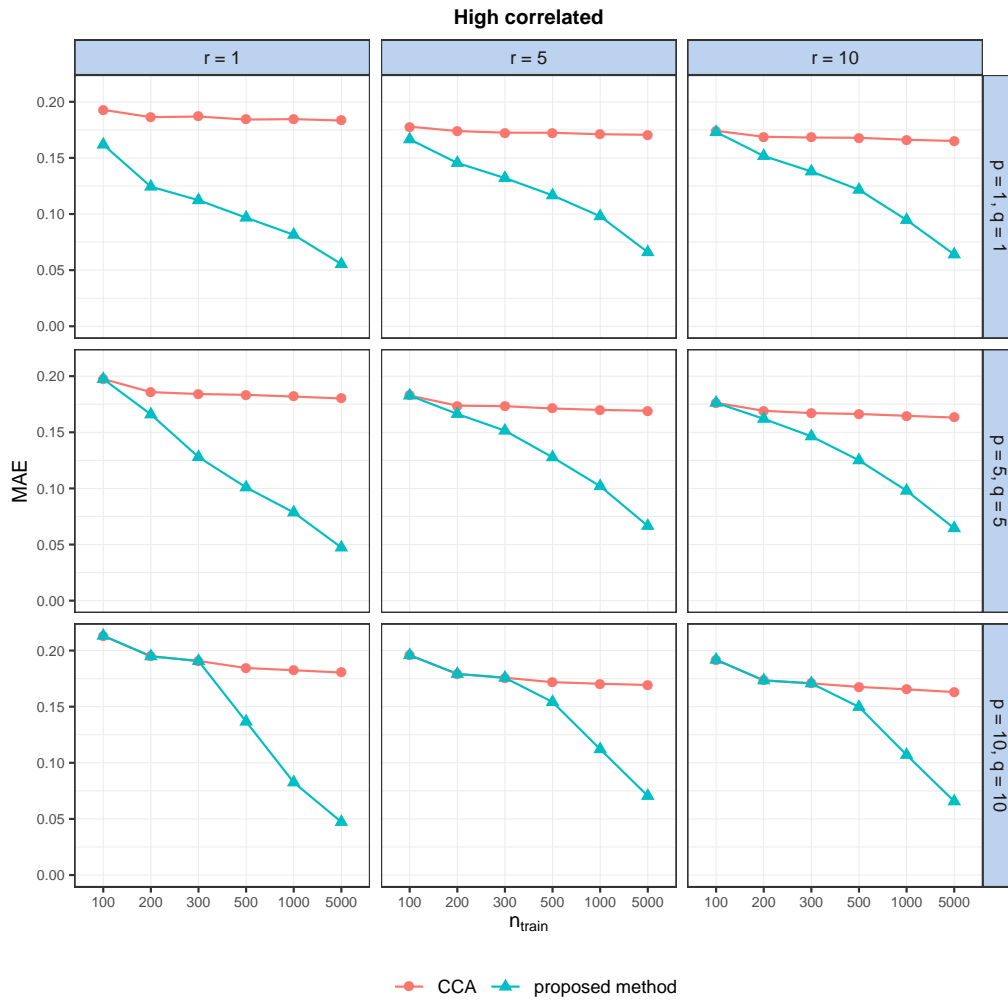


Figure 9: Performance evaluation results for high correlated data sets when $\text{nodesize} = 6 \times (p + q)$. CCA is the benchmark method. Smaller values of MAE are better.

6 EEG data

In this section, the data collection process and preprocessing steps are explained.

6.1 Neuropsychological scale

To evaluate the intellectual disabilities, performance IQ (pIQ) and verbal IQ (vIQ), which are the scores for total IQ, were obtained using the Mullen, the WPPSI-IV, the WISC-V, and the WAIS-IV batteries depending on the age of the participant. The administration was adapted for the clinical participants by starting at the first item rather than the starting point for their chronological age, frequent breaks were proposed, and participants were motivated through many creative incentives if necessary (songs, games, conversations about their interests, etc.).

6.2 EEG auditory task

The auditory task was prepared using E-prime 2.0 software (Psychology Software Tools Inc., Pittsburgh, PA, USA) on a screen placed at a viewing distance of 60 cm. Sounds, which are presented binaurally and simultaneously, were delivered through two speakers located laterally at 30 cm from the participants' ears. The auditory stimulus consisted of 24 dB/octave white noise burst. Each stimulus lasted 50 ms with an inter-stimulus interval varying between 1200 and 1400 ms to avoid a process of habituation. The task was composed of 150 trials. The total task duration was around 4 minutes. To assure maximal collaboration, a movie without sound and subtitles was presented. The participant was told to focus his/her attention on the movie and not to give attention to the auditory stimuli.

6.3 EEG recordings

The subject was placed in an electrically shielded room in the Sainte Justine's Hospital. The continuous EEG was recorded with a high-density EEG system containing 128 electrodes placed according to the extended 10 - 20 system (Electrical Geodesics System Inc., Eugene, OR, USA). Signals were acquired and processed by a G4 Macintosh computer using NetStation EEG Software (Version 2.0). Before recording, impedances were verified and were kept below 40 k Ω (Tucker, 1993). EEG data were amplified, band-pass-filtered 0.1–4000 Hz, and sampled at 1000 Hz with a vertex reference.

6.4 Preprocessing for the analysis

Off-line signal processing and ERP analyses were performed using the EEGLAB toolbox via custom Matlab scripts (Delorme and Makeig, 2004). EEG acquired data was subjected to the following pre-processing steps. First, EEG signals were digitally filtered with a high-band pass filter (0.5 Hz) and a 60 Hz notch filter. Twenty-eight electrodes placed on the neck and the face and containing muscular artifacts have been removed to avoid contamination of average reference. Moreover, a voltage threshold method (2–200 μV) was applied to exclude channels with artifacts. Data were off-line re-referenced to the mean of the EEG selected electrodes (100 channels). Independent component analysis (ICA) as implemented in the EEGLAB toolbox (with default parameters) was used to remove ocular artifacts. By removing or minimizing the effects of overlapping components, ICA enables a detailed examination of the separate dynamics of electrical brain activity as well as artifacts to remove them (Delorme *et al.*, 2007). Ocular and cardiac ICA components (range across subjects: 1–3 components) were identified by visual inspection and deleted from the global signal. Continuous EEG was segmented into epochs covering a time window from -200 ms to 800 ms relative to the onset of the tone. Also, as the artifact ICA components could be deemed unsatisfactory, the segmented EEG recordings were visually inspected by a well-trained experimenter, and trials presenting with residual artifacts were rejected.

For time-frequency (TF) and inter-trial coherence (ITC) analyses, segments were exported to MATLAB (version R20174b) (The MathWorks Inc., Natick, MA, USA) after artifact rejection. TF and ITC analyses were processed using the EEGLAB toolbox (v.13.6.5b) (La Jolla, CA, USA). TF analysis allows us to explore different frequency bands in terms of their power and temporal distributions (Herrmann *et al.*, 2005). We used complex Morlet’s wavelet transformation (Tallon-Baudry and Bertrand, 1999) to provide power maps in time and frequency domains. The simplified mathematical expression for applying this specific wavelet convolution on our EEG signal is as follows:

$$M(t, f) = \int_t W\left(\frac{t-a}{b}, f\right) S(t) dt$$

where $M(t, f)$ is a matrix of complex values (vectors) for a given time (t) and frequency (f), S is the signal as a function of time (t) and W corresponds to Morlet’s wavelet which is a complex exponential (Fourier) with a Gaussian envelope that undergoes a series of translations (a) and dilations (b) dependently of the frequency (f). The event-related

spectral perturbation (ERSP) computation uses the complex values (amplitude and phase) given by Morlet’s wavelet transform as shown in the following formula calculating the power spectrum for each time and frequency point:

$$P(t, f) = 10 \log_{10} |M(t, f)|^2$$

where $P(t, f)$ denotes TF power in terms of decibels (dB). Final TF maps were computed as follows:

$$TF = \frac{1}{N} \sum_{n=1}^N P(t, f)$$

where N is the total number of trials. The range of frequency investigated was from 3 to 100 Hz. ITC, analogous to phase-locking value (PLV), allows the assessment of the strength of phase coherence across trials in temporal and spectral domains (Makeig *et al.*, 2004). The ITC computation uses only the phase of the complex values given by Morlet’s wavelet transform. ITC was computed as in Lachaux *et al.* (1999) to extract PLV. ITC measures phase coupling across trials at all latencies and frequencies and is defined by:

$$ITC = \frac{1}{N} \left| \sum_{n=1}^N \exp(j\theta(f, t, n)) \right|$$

where θ represents the phase for a given frequency (f), time point (t), and trial (n). The obtained values are always defined between 0 and 1. Phase-locking values close to 1 indicate strong inter-trial phase-locking, thus representing evoked activity while scores closer to 0 indicate a high inter-trial phase variability, thus representing induced activity (Lachaux *et al.*, 1999).

6.5 SHAP interaction effect between age and vIQ

As mentioned in Section 4 of the paper, Figure 10 presents the interaction effect between age and vIQ. Similar to the interaction effect between sex and pIQ (right plot in Figure 8 of the paper), we see that the impact increases as we move away from the average vIQ. Again, the impact of the interaction on the theta-gamma co-variation is positive for high IQ females and negative for low IQ females whereas the opposite is observed in males.

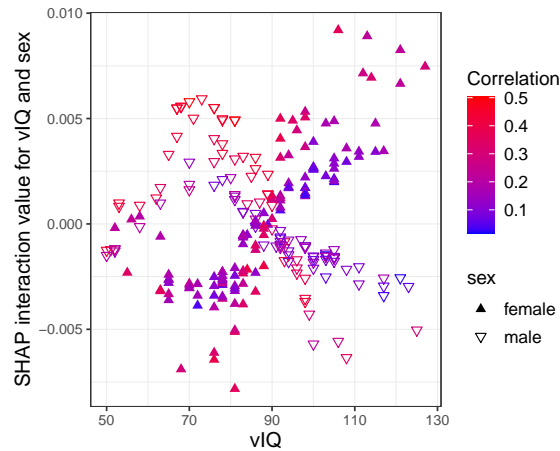


Figure 10: SHAP interaction values for sex and vIQ variable.

References for Supplementary Material

- Bach, F. R. and Jordan, M. I. (2002). Kernel independent component analysis. *Journal of machine learning research*, **3**(Jul), 1–48.
- Björck, Å. and Golub, G. H. (1973). Numerical methods for computing angles between linear subspaces. *Mathematics of computation*, **27**(123), 579–594.
- Branco, J. A. *et al.* (2005). Robust canonical correlations: A comparative study. *Computational Statistics*, **20**(2), 203–229.
- Breiman, L. (2001). Random forests. *Machine learning*, **45**(1), 5–32.
- Delorme, A. and Makeig, S. (2004). Eeglab: an open source toolbox for analysis of single-trial eeg dynamics including independent component analysis. *Journal of neuroscience methods*, **134**(1), 9–21.
- Delorme, A. *et al.* (2007). Enhanced detection of artifacts in eeg data using higher-order statistics and independent component analysis. *Neuroimage*, **34**(4), 1443–1449.
- Do Q, L. (2012). Numerically efficient methods for solving least squares problems.
- Ewerbring, L. M. *et al.* (1990). Canonical correlations and generalized svd: applications and new algorithms. In *Advances in Parallel Computing*, volume 1, pages 37–52. Elsevier.

- Golub, G. H. (1969). Matrix decompositions and statistical calculations. In *Statistical computation*, pages 365–397. Elsevier.
- Hardoon, D. R. *et al.* (2004). Canonical correlation analysis: An overview with application to learning methods. *Neural computation*, **16**(12), 2639–2664.
- Healy, M. (1957). A rotation method for computing canonical correlations. *Mathematics of Computation*, **11**(58), 83–86.
- Herrmann, C. S. *et al.* (2005). Eeg oscillations and wavelet analysis. *Event-related potentials: A methods handbook*, pages 229–259.
- Hotelling, H. (1936). Relations between two sets of variates. *Biometrika*, **28**(3/4), 321–377.
- Ishwaran, H. (2007). Variable importance in binary regression trees and forests. *Electronic Journal of Statistics*, **1**, 519–537.
- Lachaux, J.-P. *et al.* (1999). Measuring phase synchrony in brain signals. *Human brain mapping*, **8**(4), 194–208.
- Makeig, S. *et al.* (2004). Mining event-related brain dynamics. *Trends in cognitive sciences*, **8**(5), 204–210.
- Tallon-Baudry, C. and Bertrand, O. (1999). Oscillatory gamma activity in humans and its role in object representation. *Trends in cognitive sciences*, **3**(4), 151–162.
- Tucker, D. M. (1993). Spatial sampling of head electrical fields: the geodesic sensor net. *Electroencephalography and clinical neurophysiology*, **87**(3), 154–163.
- Wilms, I. and Croux, C. (2015). Sparse canonical correlation analysis from a predictive point of view. *Biometrical Journal*, **57**(5), 834–851.